Stem Cell Reports
Article

ISSCR

OPEN ACCESS

Schwann Cell Precursors from Human Pluripotent Stem Cells as a Potential Therapeutic Target for Myelin Repair

Han-Seop Kim,[1] Jungwoon Lee,[1] Da Yong Lee,[2] Young-Dae Kim,[1] Jae Yun Kim,[1,3] Hyung Jin Lim,[1,3] Sungmin Lim,[1,3] and Yee Sook Cho[1,3,*]

[1]Stem Cell Research Laboratory, Immunotherapy Convergence Research Center
[2]Rare Disease Research Center
Korea Research Institute of Bioscience and Biotechnology, 125 Gwahak-ro, Yuseong-gu, Daejeon 34141, Republic of Korea
[3]Department of Bioscience, KRIBB School, University of Science & Technology, 113 Gwahak-ro, Yuseong-gu, Daejeon 34113, Republic of Korea
*Correspondence: june@kribb.re.kr
http://dx.doi.org/10.1016/j.stemcr.2017.04.011

SUMMARY

Schwann cells play a crucial role in successful nerve repair and regeneration by supporting both axonal growth and myelination. However, the sources of human Schwann cells are limited both for studies of Schwann cell development and biology and for the development of treatments for Schwann cell-associated diseases. Here, we provide a rapid and scalable method to produce self-renewing Schwann cell precursors (SCPs) from human pluripotent stem cells (hPSCs), using combined sequential treatment with inhibitors of the TGF-β and GSK-3 signaling pathways, and with neuregulin-1 for 18 days under chemically defined conditions. Within 1 week, hPSC-derived SCPs could be differentiated into immature Schwann cells that were functionally confirmed by their secretion of neurotrophic factors and their myelination capacity in vitro and in vivo. We propose that hPSC-derived SCPs are a promising, unlimited source of functional Schwann cells for treating demyelination disorders and injuries to the peripheral nervous system.

INTRODUCTION

During their development, Schwann cells (SCs) exist as Schwann cell precursors (SCPs), immature non-myelinating SCs, and mature myelinating SCs (Jessen and Mirsky, 2005). As a major type of glial cell in the peripheral nervous system (PNS), SCs function in myelin-sheath formation, nerve impulse transmission, and the secretion of a variety of neurotrophic factors, such as brain-derived neurotrophic factor (BDNF), glial cell-derived neurotrophic factor (GDNF), nerve growth factor (NGF), and neurotrophin-3 (NT-3), and extracellular matrix components that provide a beneficial microenvironment for neuronal survival and axonal growth (Ndubaku and de Bellard, 2008). Transplanted SCs can myelinate PNS as well as CNS axons and contribute to improving or restoring conduction and function in demyelinated axons (Golden et al., 2007; Levi et al., 1994); thus, human SCs (hSCs) represent one of the most promising targets for the development of effective treatments for PNS and CNS injuries.

Autologous primary hSCs are highly desirable for disease modeling, phenotypic drug discovery, and treating nerve injuries, but their utility is restricted by limitations such as insufficient numbers of cells due to their low division rate and fibroblast contamination over time in in vitro culture, as well as by technical issues related to isolation and purity (Rutkowski et al., 1995; Xu et al., 2008). For large-scale production, primary SC-like immortalized hSC lines have been established using the SV40 large T-antigen and human telomerase reverse transcriptase expression vectors, and their potential for use in drug development has been suggested (Lehmann et al., 2012). In addition, progress in stem cell research has contributed to expanding the feasible sources of hSCs to include not only neural crest stem cells (NCSCs) (Al-Zer et al., 2015; Ren et al., 2013; Sakaue and Sieber-Blum, 2015), but also a broad range of tissue-specific adult stem cells such as skin-derived precursors (Chen et al., 2012; Krause et al., 2014; McKenzie et al., 2006), adipose-derived stem cells (Razavi et al., 2015; Tomita et al., 2013), dental pulp stem cells (Martens et al., 2014), muscle-derived stem cells (Lavasani et al., 2014), and umbilical cord blood mesenchymal stem cells (Xiao and Wang, 2015). In another approach, hSCs can also be produced from transient neural precursors that are converted from human fibroblasts using cellular reprogramming via treatment with small-molecule inhibitors of multiple kinases, specifically AMPK, PKA, MSK1, SGK1, ROCK2, and PKGa (Thoma et al., 2014).

Currently, much attention has been paid to human pluripotent stem cells (hPSCs), including human embryonic stem cells (hESCs) and human induced pluripotent stem cells (hiPSCs), due to their excellent abilities to differentiate into many cell types, including in particular a wide variety of neural crest derivatives. The hSCs can be indirectly induced by a stepwise in vitro continuous differentiation protocol of hPSCs via an induction of multipotent NCSCs (Lee et al., 2010; Liu et al., 2014; Ziegler et al., 2011). Lineage-specific differentiation of hPSCs into NCSCs can be achieved by pharmacological modulation of key signaling pathways in neural crest development,

specifically by the inhibition of both transforming growth factor β (TGF-β) signaling and BMP-dependent Smad signaling in combination with the activation of Wnt signaling (Kreitzer et al., 2013; Menendez et al., 2011). To increase the differentiation efficiency, hPSC-differentiated NCSCs (hPSC-NCSCs) can be purified by fluorescence-activated cell sorting (FACS) for the neural crest marker nerve growth factor receptor (NGFR) and then expanded for seven passages (Liu et al., 2014). The functionality of hSCs derived from hPSC-NCSCs in vitro has been determined by their myelination capacity as evaluated using a dorsal root ganglion (DRG) neuron-SC co-culture system (Liu et al., 2012; Ziegler et al., 2011). However, such approaches still suffer from a low yield and purity of the differentiated SCs, a complicated and time-consuming differentiation process, and a lack of functionality.

SCPs represent distinct intermediate cells between migrating neural crest cells and immature pre-myelinating SCs at an early developmental stage in the SC lineage (Dong et al., 1999; Jessen et al., 1994), and are considered the most favorable source for the directed production of SCs. However, hPSC-derived SCPs (hPSC-SCPs) have rarely been studied. Here, we report an effective protocol for producing self-renewing SCPs from hPSCs. Our stepwise differentiation protocol begins by using a combination of two small molecules, SB431542 (a TGF-β inhibitor) and CT99021 (a glycogen synthase kinase-3 [GSK-3] inhibitor), followed by additional treatment with neuregulin-1 (NRG1), and it yields high-quality multipotent SCPs. hPSC-SCPs can be expanded and cryopreserved without losing their proliferative and differentiation potential. The in vitro-expanded hPSC-SCPs are efficiently capable of maturing into functional SCs within a week, as demonstrated by their secretion of neurotrophic factors, such as GDNF, NGF, BDNF, and NT-3, and their ability to myelinate rat DRG axons in vitro. Importantly, SC transplants enhanced axonal regeneration in sciatic nerve-injured mice. Collectively, our results suggest that hPSC-SCPs are a valuable source for myelin-forming SCs, and these cells may eventually provide greater insights into the pathogenesis of nerve injury and neuropathy and provide an invaluable platform for therapeutic strategies.

RESULTS

Directed Differentiation into SCPs from hPSCs

NCSCs, which are differentiated from hPSCs via neural intermediates, have been proposed as a useful source for SC production (Lee et al., 2010; Liu et al., 2014), but there are limitations to their usefulness, specifically the absence of simple, inexpensive, quick, and efficient methods. Here, we explore whether lineage-restricted SCPs, which function as an intermediate precursor between NCSCs and SCs, can be directly generated from hPSCs, potentially allowing the omission of the NCSC differentiation step. Such a protocol would decrease the time required for SC differentiation and enhance their efficiency and, ultimately, functionality. As the first step, H9 hESCs cultured in mTeSR-defined medium were neuralized for 6 days in a modified neural differentiation medium (NDM) containing SB431542 (a specific inhibitor of the TGF-β/Activin/Nodal pathway) and CT99021 (a specific inhibitor of GSK-3) (Li et al., 2011; Smith et al., 2008) to form neural rosettes (D-6 to D0) (Figure S1A). In the second step, the cells were further converted into SCPs by the simple addition to NDM of NRG1, which is known as a key factor for SC differentiation and proliferation (Birchmeier and Nave, 2008; Krishnan, 2013), and they were routinely passaged when they reached 90% confluence (Figure 1A) (D0 to D18). On day 18 of differentiation, differentiated SCPs formed highly homogeneous cell populations and displayed a high proliferative capacity with a doubling time of approximately 30 hr (Figure 1A). The induction of SCPs was evaluated and defined based on the cell morphology and expression of lineage-specific markers, as analyzed by real-time qPCR and immunocytochemistry. In the second differentiation step, the cells became elongated with a slender shape. At approximately day 5 of the second differentiation step, expression of the marker genes for NCSC (*PAX3, TWIST,* and *SLUG*), NCSC/SCP (*FOXD3, NGFR,* and *SOX10*), and SCP (*CDH19, GAP43,* and *MPZ*) lineages were significantly upregulated, and their expression peaked at different time points (Figure 1B). The expression levels of the NCSC marker genes *PAX3, TWIST,* and *SLUG* were transiently upregulated at earlier differentiation time points, with peak expression at days 5 and 10, respectively. Importantly, expression of the SCP-specific marker genes *CDH19, MPZ,* and *GAP43* peaked at approximately day 18 and maintained peak levels during subsequent prolonged culture (Figure 1B). Immunocytochemistry analysis performed in parallel confirmed the positive expression of the SCP markers SOX10 and GAP43 (Figure 1C). FACS analysis showed that more than 99% of all cells were positive for SOX10 at day 18, with SOX10 expression persisting during culture (Figure 1D). In addition to H9 hESCs, the differentiation potential into SCPs was also confirmed in the other hESC lines H1 and H7 (Figures S1B and S1C). In our protocol, omission of any of the differentiation components, NRG1, SB431542, or CT99021, led to a failure to differentiate into SCPs (Figures S1D and S1E). We note that NRG1 increased the SOX10-positive cell populations in a dose-dependent manner during the second differentiation step (Figures S1F and S1G), suggesting that activation of the NRG1 signaling pathway played a critical role in the cell fate decision to produce SCPs from neurally converted

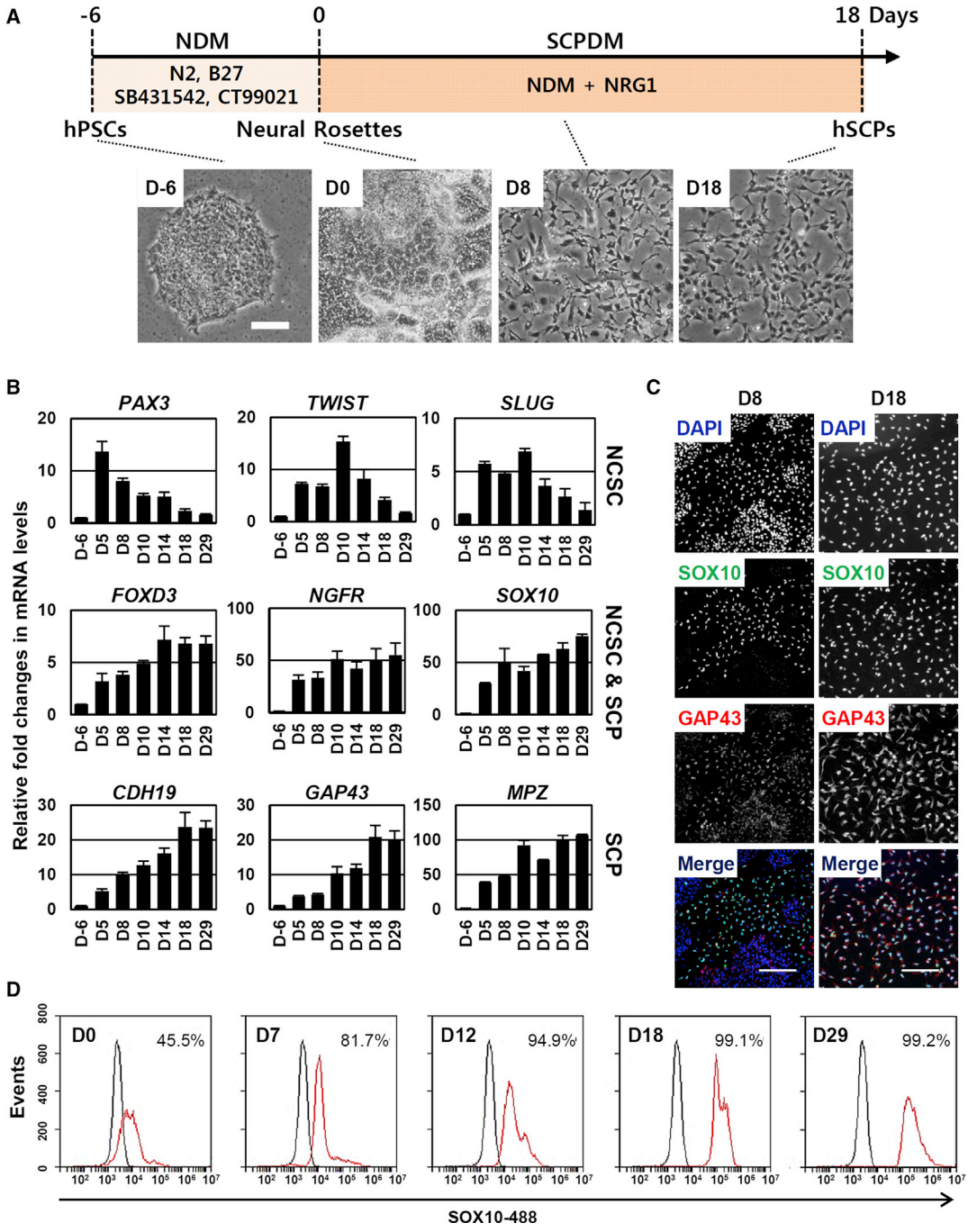

Figure 1. Directed Differentiation of hPSCs into hSCPs

(A) Schematic representation of the differentiation of hPSCs into SCPs. H9 hESCs were differentiated into neural rosettes by treatment with neural differentiation medium (NDM) for 6 days. The cells in the neural rosettes were re-plated on day 0 and further maintained in Schwann cell precursor differentiation medium (SCPDM). Bottom, representative bright-field images showing the process of differentiation into hSCPs. Scale bar, 100 μm.

(B) qPCR analysis of NCSC-specific (*PAX3, TWIST,* and *SLUG*), NCSC- and SCP-specific (*FOXD3, NGFR,* and *SOX10*), and SCP-specific markers (*CDH19, GAP43,* and *MPZ*) during differentiation into hSCPs. Mean ± SE (n = 3 independent experiments). All values are relative to hESCs (day −6).

(C) Immunocytochemical staining for SOX10 (green) and GAP43 (red) at differentiation days 8 and 18. DAPI (blue) was used to stain the cell nuclei. Scale bars, 100 μm.

(D) Flow cytometric analysis was used to estimate the number of cells expressing SOX10 during the generation of SCPs.

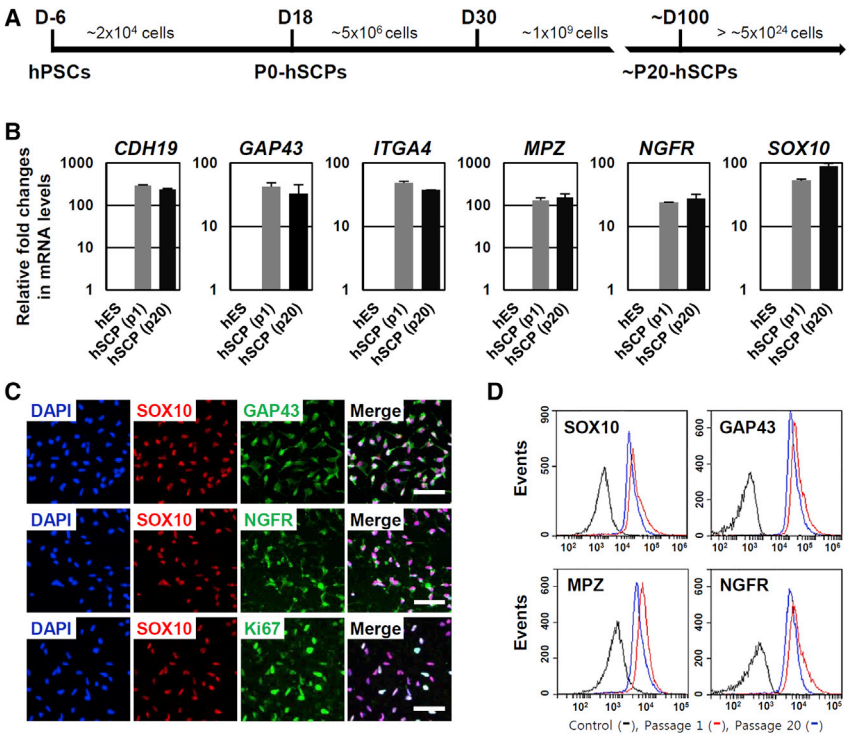

Figure 2. hSCPs Are Expandable and Can Be Maintained over Long-Term Culture

(A) Schematic representation of the differentiation of hPSCs into hSCPs and scalable production.

(B) qPCR analysis of SCP markers (*CDH19, GAP43, ITGA4 MPZ, NGFR,* and *SOX10*) in early-passage (p1) and late-passage (p20) hSCPs from H9 hESCs. Mean ± SE (n = 3 independent experiments). All values are relative to hESCs.

(C) Immunocytochemical staining of SCP markers such as SOX10 (red), NGFR (green), GAP43 (green), and Ki67 (green) in hSCPs from H9 hESCs (passage 20). Ki67 was used as a cell proliferation marker. Cell nuclei were stained with DAPI (blue). Scale bars, 50 μm.

(D) Flow cytometric analysis of hSCP markers (SOX10, NGFR, MPZ, and GAP43) in early-passage (p1) and late-passage (p20) hSCPs from H9 hESCs.

hPSCs, which were induced by dual inhibition of the TGF-β and GSK-3 pathways.

To compare the characteristics of hESCs and hiPSCs during differentiation into SCPs at the molecular level, we used microarray analysis to explore and compare the global gene expression profiles of SCPs differentiated from hESCs (hESC-SCPs) and from hiPSCs (hiPSC-SCPs). A heatmap of the whole-gene expression profiles of both hESC-SCPs and hiPSC-SCPs showed similar gene expression patterns. As expected, SCPs from both hESCs and hiPSCs expressed relatively low levels of key pluripotency marker genes such as *POU5F1, KLF4, MYC, ZFP42, SOX2,* and *SOX1*, of NCSC-related genes such as *ZIC3, DBP, FOXC1,* and *MSX2*, and significantly higher levels of SCP marker genes such as *ITGA4, NGFR, SOX10, CDH19, DHH, GAP43,* and *MPZ* (Figure S2A). Real-time qPCR (Figure S2B) and semi-quantitative RT-PCR analysis (Figure S2C) provided results consistent with the microarray data, suggesting that our two-step differentiation from hPSCs to SCPs was successful for both hESCs and hiPSCs.

During development, SCPs are known as intermediary precursors between NCSCs and immature SCs (Adameyko et al., 2009). Characterization of lineage markers for SCPs and NCSCs clearly showed the lineage differences between differentiated SCPs and NCSCs (Figure S3A). Furthermore, microarray analysis displayed distinct differences in lineage-specific gene expression between SCPs and NCSCs from hiPSCs (Figure S3B). Consistent with the microarray data, real-time qPCR results validated that lineage marker genes specific for SCPs, such as *CDH19, SOX10, GAP43,* and *NGFR*, were highly expressed in SCPs, while *TWIST* and *SLUG*, which were specific for NCSCs, dominantly expressed in NCSCs (Figure S3C). Immunocytochemistry analysis confirmed that NCSCs were positive for SOX10 and NGFR but negative for the SCP marker *GAP43* (Figure S3D). Taken together, we provide a simple means of generating highly homogeneous SCPs from hPSCs by sequential combined treatment with SB431542 and CT99021, followed by NRG1, SB431542, and CT99021, without the need for other steps such as cell purification and medium changes under chemically defined conditions.

SCPs Are Highly Expandable and Can Be Maintained Long-Term in Defined Medium

In the presence of a high concentration of NRG1 (100 ng/mL), SCPs from hPSCs were stably expandable for more than 35 passages under chemically defined conditions without any major morphological changes or loss of SCP characteristics between the passages (Figures 2 and S4). Microarray analysis demonstrated nearly identical expression patterns of major SCP marker genes in early-passage (p1) and late-passage (p19) SCPs from hESCs and hiPSCs (Figure S4A). qPCR (Figures 2B and S4B) and semi-quantitative RT-PCR analysis (Figure S4C) also confirmed that both early-passage (p1) and late-passage (p20) SCPs stably

expressed SCP marker genes such as *CDH19, GAP43, ITGA4, MPZ, NGFR,* and *SOX10*. Consistently, immunocytochemistry analysis showed that both early-passage (Figure 1C) and late-passage SCPs (p20) were positive for Ki67 (more than 95%), a marker of proliferating cells, and uniformly expressed the SCP marker proteins GAP43, NGFR, and SOX10 (Figure 2C). Flow cytometric analysis showed similar expression levels of SCP-specific markers, such as *SOX10, NGFR, GAP43,* and *MPZ*, between early- and late-passage SCPs (Figure 2D), indicating that cultured SCPs were self-renewable and homogeneous in a chemically defined medium. The SCPs derived from either hESCs or hiPSCs could be successfully cryopreserved by conventional methods and were recovered after thawing and reculturing. Taken together, we provide a simple means of generating highly homogeneous SCPs from hPSCs under chemically defined conditions without the need for further cell purification.

Multipotent SCPs Efficiently Differentiate into Schwann Cells

Although little is known about the signaling molecules that convert SCPs into immature SCs, SC differentiation is known to be influenced by cAMP concentration (Bacallao and Monje, 2013; Monje et al., 2008, 2010). In fact, rodent immortalized SCPs were induced to differentiate into the SC lineage by treatment with forskolin, a PKA activator (Lobsiger et al., 2001). NRG1 and cAMP act cooperatively not only to promote SCP survival and proliferation but also to accelerate the differentiation of SCPs into SCs (Brennan et al., 2000; Woodhoo and Sommer, 2008). Based on such approaches, we have successfully optimized the differentiation protocol to generate SCs from hPSC-SCPs using SC differentiation medium (SCDM) containing NRG1 (200 ng/mL), retinoic acid (RA) (100 nM), platelet-derived growth factor-BB (PDGF-BB) (10 ng/mL), and forskolin (4 μM). After approximately 4–8 days of differentiation with SCDM, H9-SCPs shifted to exhibiting a bipolar spindle-like morphology (Figures 3A and S5A) accompanied by a significant increase in the expression levels of SC markers (such as *GFAP, PLP, PMP22,* and *S100*) (Figure 3B) and various neurotrophic factors (such as *BDNF, GDNF, NGF, NT-3, NT-4,* and *CNTF*) (Figure S5B). The average time to acquiring the SC identity was approximately 7 days, as determined by the cell morphology and expression profiles of SC markers. Differentiated SCs expressed high levels of the major neurotrophic factor genes (*NGF, BDNF,* and *GDNF*) and of markers of immature SCs (*S100B, NGFR, MPZ, PMP22*, *OCT6*, and *SOX10*) (Figure 3C). In addition, immunocytochemical analysis showed that the most differentiated SCs were positive for SC lineage-specific proteins such as S100B, NGFR, EGR2, and MPZ (Figure 3D). We also confirmed that H1-SCPs and H7-SCPs differentiated into SCs using the above protocol (Figure S5C). A heatmap (6804 significant transcripts, t test, $p < 0.01$) of the microarray data showed that hPSC-SCP-derived SCs and primary hSCs were very similar, whereas SCs from either source were clearly distinguished from SCPs (Figure 3E). Although SCPs were originally identified as glial-restricted progenitors that only differentiated into SCs in PNS (Dong et al., 1999; Jessen et al., 1994), recent reports have suggested that these cells are multipotent and could differentiate into varied cell types, including parasympathetic neurons and melanocytes (Adameyko et al., 2009; Dyachuk et al., 2014; Espinosa-Medina et al., 2014; Jessen and Mirsky, 2005). Thus, we further tested the capacity of hPSC-derived SCPs to generate melanocytes. During the differentiation of hESC-derived SCPs into melanocytes, the expression levels of melanocyte marker genes, specifically *TYROSINASE, MITF,* and *TYRP1*, increased gradually over time (Figures S5D and S5E), and, after 16 days of differentiation, most of the cells were positive for melanocytic markers such as MITF and MelA (Figure S5F) and were pigmented (Figure S5G). Furthermore, we performed a clonal analysis and confirmed that individual clones were proliferative and able to directly differentiate into SCs or melanocytes under the respective differentiation conditions (data not shown). These findings suggest that hPSC-SCPs are multipotent and have the properties of authentic SCPs.

SCP-Derived Schwann Cells Are Functional Both In Vitro and In Vivo

We next addressed the functionality of SCs derived from hPSC-SCPs by confirming their potential to myelinate peripheral neuronal axons in vitro. The hPSC-SCP-SCs were co-cultured with embryonic rat DRG neurons in the presence of myelination-promoting ascorbic acid in 12- or 24-well plates. After induction of myelination, mixed cultures were immunostained for myelin basic protein (MBP), indicating myelin segments, and for neuron-specific tubulin (TUJ-1) (Figure 4A). Under our co-culture condition, 28 days after inducing myelination, the presence of MBP-positive myelin segments was confirmed (1.5 myelin segments per well of a 12-well plate, n = 16) (Figure 4A). Residual rat SCs were not myelinated, as visualized by labeling myelinating cells with human-specific nuclear antibody (Figure 4A). Most of the co-cultured hPSC-SCP-SCs were immunostained for S100B and aligned with neurofilament-positive DRG axons (Figure 4B). MPZ-positive myelinating hPSC-SCP-SCs co-localized with neurofilament-positive DRG axons (Figure 4C). SCs function not only in axonal myelination but also in providing trophic factors for axonal regeneration. Real-time qPCR analysis showed that neurotrophic factors, such as *BDNF, GDNF, NGF,* and *NT-3*, were highly expressed in hPSC-SCP-SCs (Figure S5B). Significantly, the ELISA results showed that the levels of

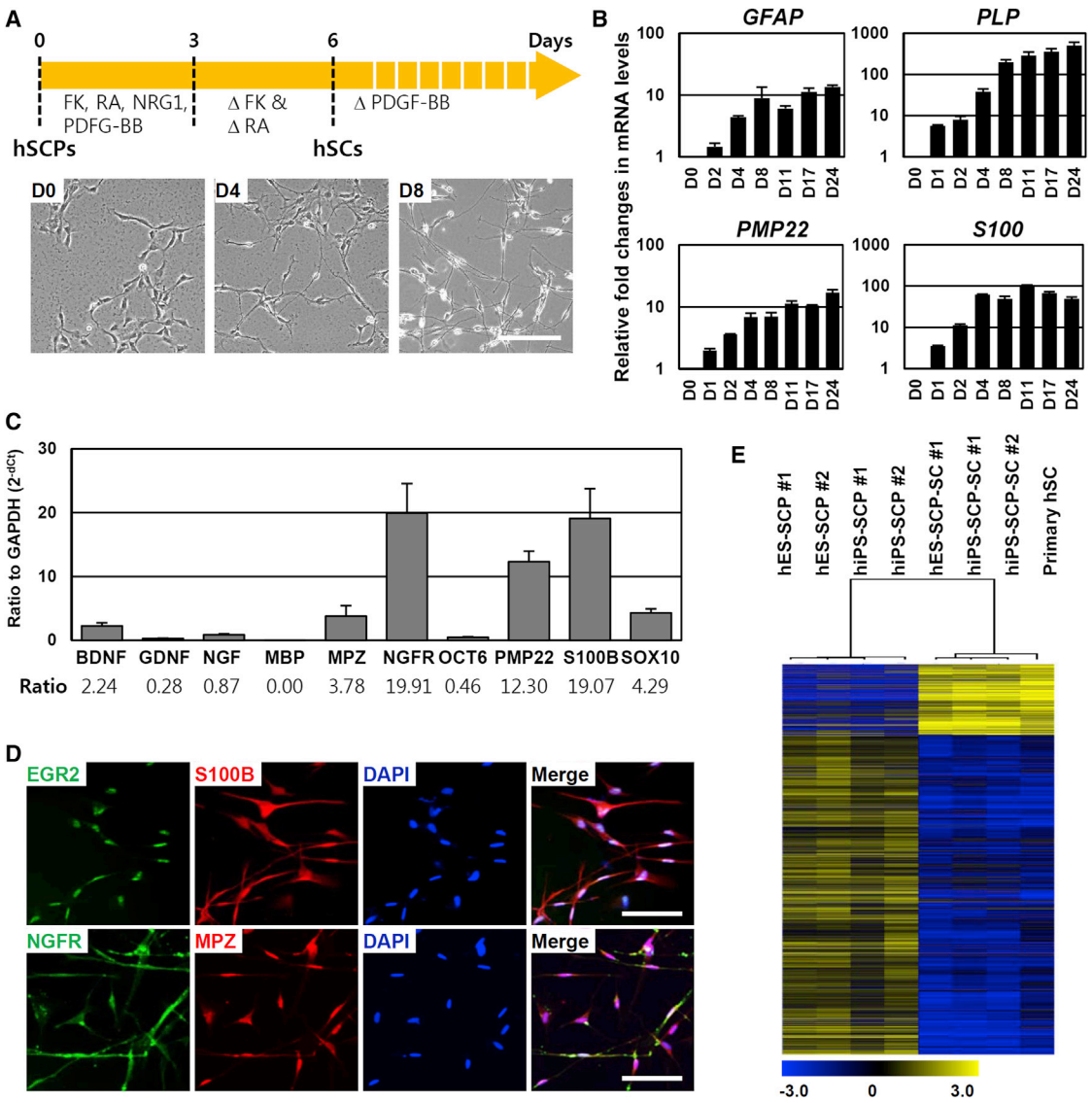

Figure 3. hSCPs Can Rapidly and Efficiently Differentiate into Schwann Cells

(A) Schematic representation of the differentiation of hSCPs into Schwann cells. Bottom, representative phase-contrast images of cells during differentiation into hSCP-SCs. Scale bar, 200 μm.

(B) qPCR analysis of the Schwann cell marker genes *GFAP, PLP, PMP22,* and *S100* during the differentiation of H9-SCPs into hSCP-SCs. Mean ± SE (n = 3 independent experiments). All values are relative to H9-SCPs.

(C) qPCR analysis of neurotrophic factors (*BDNF, GDNF,* and *NGF*) and Schwann cell marker genes (*MPZ, MBP NGFR, PMP22, S100,* and *SOX10*) in hSCP-derived Schwann cells obtained after 10 days of differentiation. The ratio of the mRNA expression level of the indicated gene versus GAPDH was defined as 2^{-dCt}. Mean ± SE (n = 5 independent experiments).

(D) Immunostaining for the Schwann cell markers NGFR (green), S100 (red), EGR2 (green), and MPZ (red) after 10 days of differentiation. Cell nuclei were stained with DAPI (blue). Scale bars, 100 μm.

(E) Microarray analysis was used to compare the gene expression levels in hSCPs with those in hSCP-SCs and in primary hSCs. The heatmap shows the relative value of the log10 fold-change based on the value in undifferentiated H9 hESCs.

secreted BDNF, GDNF, NGF, and NT-3, which are known as crucial factors for axonal regeneration in both PNS and CNS, were higher in hPSC-SCP-SC culture medium than in the culture medium of undifferentiated SCPs (Figure 4D).

To test the in vivo functionality of hPSC-SCP-SCs, SCs labeled with GFP were transplanted into mice subjected to a sciatic nerve injury model (Figure 5A). Sciatic nerve regeneration from proximal stumps to a distal location

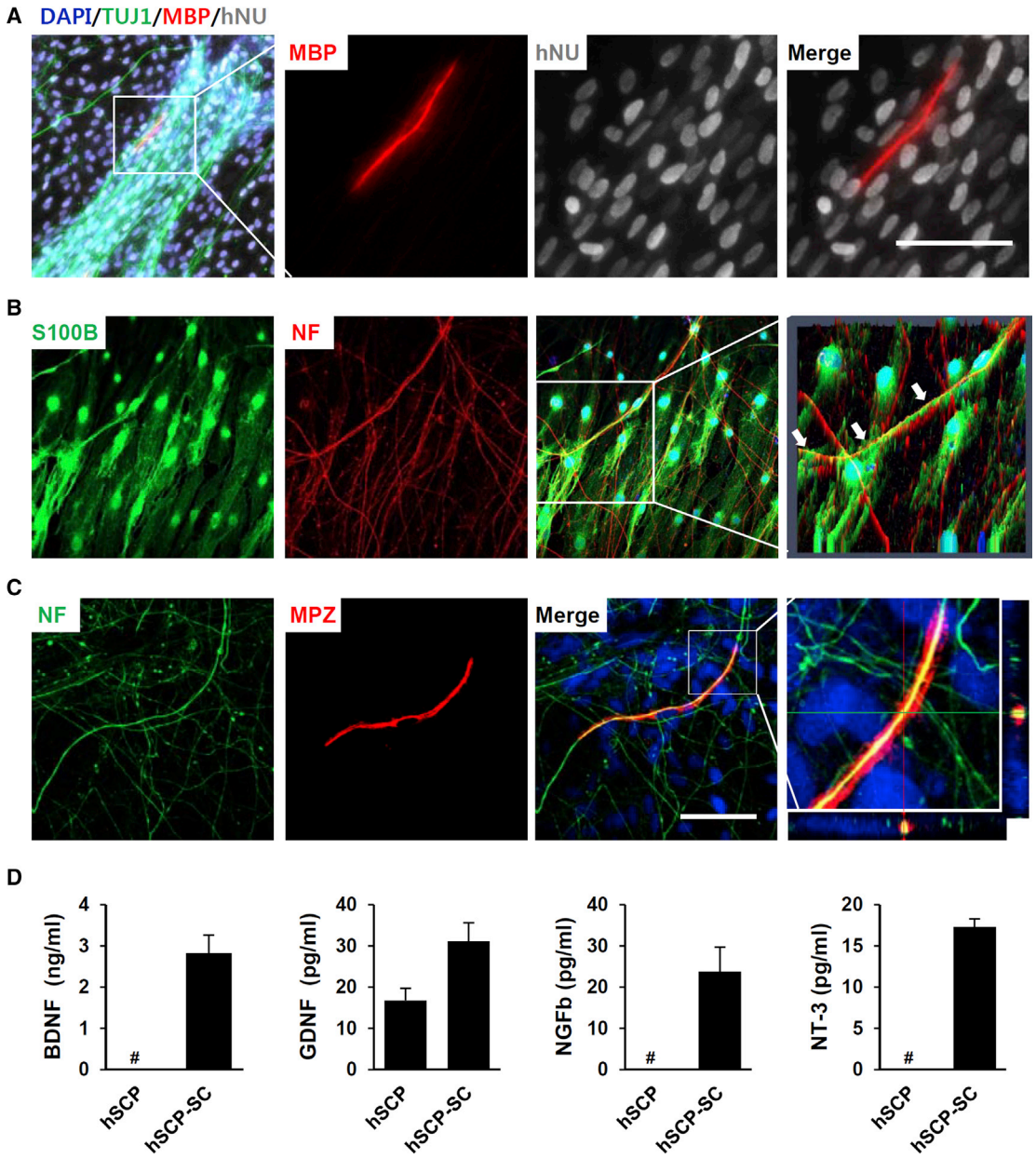

Figure 4. hSCP-Derived Schwann Cells Were Myelinated and Secreted Neurotrophic Factors

(A) The Schwann cells differentiated from H9-SCPs were co-cultured with rat DRGs for 28 days and then immunostained for MBP (red), TUJ1 (green), and human nuclear (hNU, gray). A higher magnification of the boxed area shows that the hNU-positive cell co-stained with MBP. Scale bar, 50 μm.

(B) Most of the unmyelinated-Schwann cells were immunostained with S100B, a Schwann cell marker. Cell nuclei were stained with DAPI (blue) in merged image. Arrows in the higher magnification of the boxed area of a 2.5D reconstruction using Zen software show that the Schwann cells contained aligned neurofilaments (NF).

(C) Orthogonal reconstruction of the boxed area showing DAPI (blue) was used to stain the cell nuclei in a merged image. MPZ-positive cells with strong immunoreacitivity for MPZ were surrounding the NF. The slice thickness was 0.34 μm. Scale bar, 50 μm.

(D) ELISA showing that the levels of neurotrophic factors known to be secreted by Schwann cells, such as BDNF, GDNF, NGF, and NT-3, were significantly increased after 18 days post-differentiation from H9-SCPs to H9-SCP-SCs. Mean ± SE (n = 2 independent experiments). Data were run in duplicate, and the experiments were performed twice. #, no detection of neurotrophic factor.

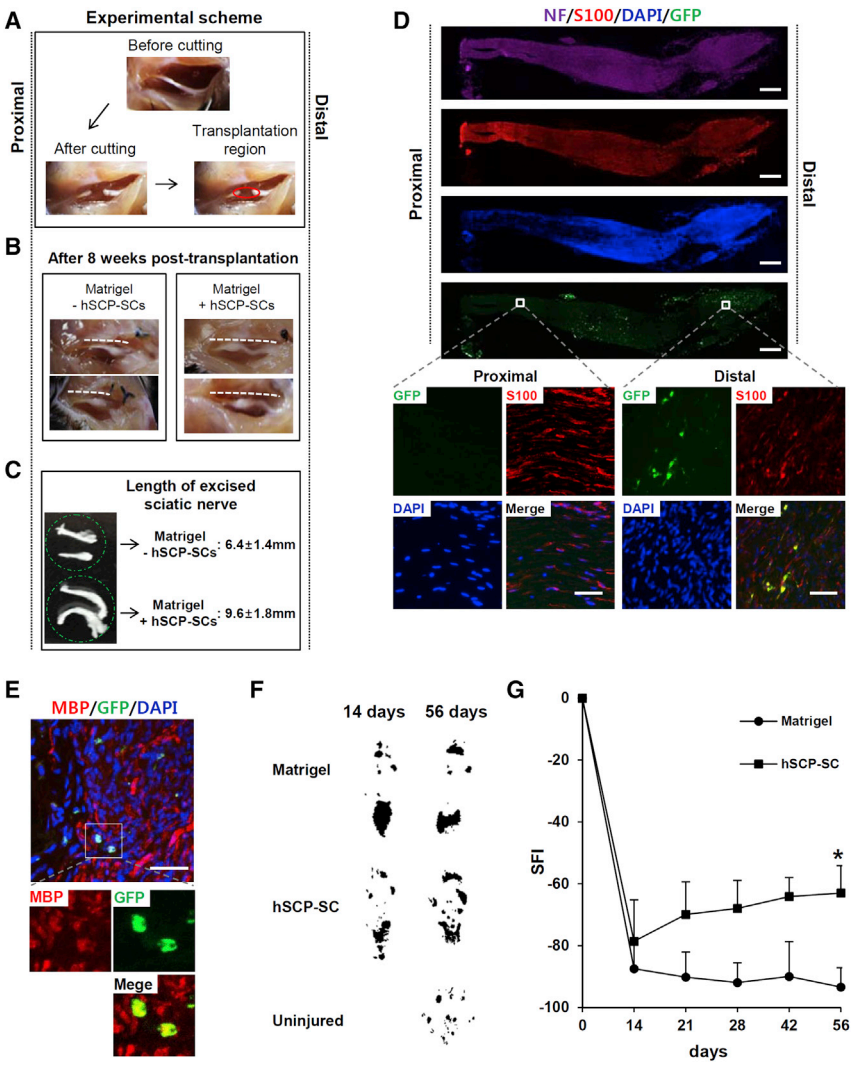

Figure 5. hSCP-Derived Schwann Cells Promoted Peripheral Nerve Regeneration In Vivo

(A) Experimental scheme. Eight-week-old male mice were used for the sciatic nerve injury model. Five microliters of Matrigel or Matrigel plus SCP-SC mixture was transplanted into the region of injury (red circle).

(B) Representative image of sciatic nerve regeneration after hSCP-derived Schwann cell transplantation into the region of the damaged nerve 8 weeks after injury (dotted line; sciatic nerve).

(C) The length of the excised sciatic nerve was measured using a ruler at 8 weeks after injury. Mean ± SE (n = 12 mice per group).

(D) Longitudinal section of sciatic nerve induced to regenerate by GFP-labeled hSCP-SC at 8 weeks after injury and immunostained for S100B (red) and NF (violet). Scale bars, 500 μm. Inset, higher-magnification image showing that grafted GFP-labeled Schwann cells survived and were immunostained with the Schwann cell marker S100B. Scale bars, 50 μm.

(E) Cross-sections showing immunostaining for MBP. Inset, higher-magnification image showing that the grafted Schwann cells were positive for MBP. Scale bars, 50 μm.

(F) Representative footprint patterns from mice transplanted with Matrigel (control) or Matrigel plus hSCP-SCs.

(G) Quantification of footprints for SFI in hSCP-SC-transplanted versus control mice at the indicated days after injury. Mean ± SE (n = 16 mice per group). *p < 0.01 when comparing control and SCP-SCs using a t test.

was observed after 8 weeks post-injury in the SC-transplanted mice (n = 20), while the sciatic nerve in the Matrigel-treated mice (n = 18) exhibited little regeneration at the same time point after injury (Figure 5B). Remarkably, 8 weeks after injury, the length of the excised sciatic nerves was significantly increased in SCP-SC-transplanted mice (9.6 ± 1.8 mm) compared with control mice (6.4 ± 1.4 mm) (Figure 5C). GFP-labeled-SCs were potentially integrated into the distal region of regenerated sciatic nerve tissues, among which the most GFP-labeled cells were immunostained with S100B (Figure 5D). Renewed axons distinguished by DAPI staining were mostly detected in the distal region (Figure 5D). The proportion of MBP-positive cells in GFP-positive cells, indicating myelination of transplanted SCP-SCs, were quantitated by counting six randomly selected fields among distal region of 60 slices obtained from three sciatic nerves and detected at a frequency of approximately 0.012% (6 MBP-positive myelinating cells in 50,000 GFP-positive cells) (Figure 5E). Eight weeks after SCP-SC-transplantation, the presence of remyelination of the axons in the distal region was further visualized by CASPR immunostaining (Figure S6A) and transmission electron microscopic examination (Figures S6B and S6C). Notably, without SCP-SC-transplantation, demyelinated axons were not remyelinated or restored (Figure S6C). These results suggest that remyelination was induced by the transplanted SCP-SCs and endogenous SCs were not potent enough to rescue the myelination defect. In addition, we confirmed the functional recovery of sciatic nerve-injured mice by obtaining footprints from the SCP-SC-transplanted mice at 2, 3, 4, 6, and 8 weeks (Figure 5F) (n = 18 or 20 mice). Compared with the Matrigel-treated control mice, SCP-SC-transplanted mice had a significantly improved sciatic function index (SFI) based

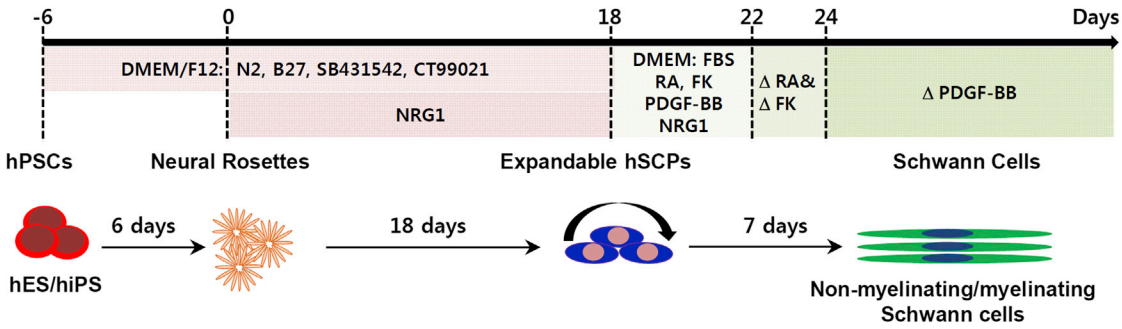

Figure 6. Scalable Generation of Highly Pure Populations of Schwann Cells from hPSCs via hSCPs

A simple protocol to generate highly homogeneous functional Schwann cells from hPSCs via self-renewable hSCPs by sequential treatment with culture medium as summarized in the figure.

on footprint measurements in the walking track analysis. These findings demonstrated a significant improvement of the functional recovery (Figure 5G). Increased SFI was observed at 2 weeks post-transplantation and further increased by 8 weeks (average SFI −62.9 ± 8.7 versus control group −93.3 ± 6.3). These results are reproducible and suggested that hPSC-SCP-SCs are functional and useful for therapeutic application for nerve regeneration.

DISCUSSION

Authentic SCPs, defined as the earliest developmental stage of the SC lineage, were primed toward SC differentiation. It may be possible to harvest them from nerve biopsies, but they are extremely challenging to obtain, maintain in an undifferentiated state, and to expand in vitro, possibly due to a limited availability of exogenous trophic factors that support the survival, identity, and functionality of SCPs. To obtain a stable source of SCPs, the conditionally immortalized rat SCP line SpL201 was established from embryonic day 14.5 sciatic nerves by the introduction of a retrovirally encoded EGFR/neu fusion protein (Lobsiger et al., 2001), but there is still no adequate methodology for continuously supplying hSCPs. Thus, we present the stepwise differentiation protocol to directly generate an unlimited supply of fate-restricted SCPs from hPSCs, and subsequently a highly pure population of functional SCs, while bypassing the need for hNCSCs (Figure 6).

Although SCs can be differentiated from hPSC-derived NCSCs (hPSC-NCSCs) (Chambers et al., 2009; Jiang et al., 2009; Lee et al., 2010), those protocols generally require many weeks or months to scale up, and they supply limited purity. Although several protocols have been shown to improve upon these hurdles, including the "LSB-short" method based on dual SMAD inhibition, which demonstrates improved yields of NCSCs and a shorter differentiation time (8 days) (Kreitzer et al., 2013), and the NCSC enrichment method using NGFR-FACS purification (Liu et al., 2014), a differentiation time of more than 40 days was still required to produce SCs from hNCSCs (Liu et al., 2014). Moreover, the functionality of SCs differentiated from hNCSCs remains limited; very few hNCSC-derived SCs give rise to functional myelinating cells (Liu et al., 2012), and little information has been reported regarding their effectiveness for axonal regeneration and recovery from peripheral nerve injury in vivo.

We focused our efforts on developing a differentiation protocol that can directly generate hSCPs from hPSCs, including both hESCs and hiPSCs, in an attempt to contribute to the supply of functional hSCs on a large scale and in a reduced time frame. During the first differentiation step for inducing SCPs, two small molecules (CT99021, GSK-3 inhibitor; and SB431542, TGF-β inhibitor), which were chosen based on the conditions of directed neural epithelium or neural crest specification (Li et al., 2011; Menendez et al., 2011), effectively worked to derive neural rosettes from hPSCs maintained in chemically defined mTeSR1 medium under adherent culture conditions and in the absence of feeder cells for 6 days. In a second step, an additional treatment with a high concentration of the SC-lineage-promoting NRG1 (over 50 ng/mL) (Birchmeier and Nave, 2008; Falls, 2003) effectively induced self-renewable, multipotent hPSC-SCPs over an additional 18 days of culture (Figures 1 and 2). Nearly all of the differentiated cells (over 99%) were homogeneous in appearance and identified as SOX10-positive hPSC-SCPs, representing a high yield and purity.

The hPSC-SCPs can be produced within a month from either hESCs or hiPSCs (Figure S4), with no notable differences in overall properties such as lineage marker expression, proliferation, and differentiation potential, under chemically defined medium, and they can be stably expanded for more than 3 months (≥35 passages) without

a loss of differentiation potential, even after cryopreservation. Multipotent SCPs can be differentiated into varied cell types derived during embryonic development, such as parasympathetic neurons and melanocytes (Adameyko et al., 2009; Dyachuk et al., 2014; Espinosa-Medina et al., 2014). Importantly, only approximately a week is required to acquire functional SC competency from hPSC-SCPs (Figures 3 and 4). In addition, hPSC-SCPs are prone to differentiation into SCs. We were able to differentiate hPSC-SCPs into melanocytes but not into neurons. Lineage-specific differences between and characteristics of SCPs and NCSCs derived from hPSCs were confirmed by comparative investigation at both the gene and protein expression levels (Figure S3) and based on functional differences in their differentiation potentials.

NRG1/ErbB signaling is known to be essential for the molecular regulation of SC development, proliferation, and differentiation (Birchmeier and Nave, 2008; Newbern and Birchmeier, 2010). The binding of NRG1 ligands to members of the ErbB2/3 family of tyrosine kinase receptors leads to the activation of complex intracellular signaling pathways, such as MAPK, phosphatidylinositol 3-kinase, or PLCγ, and subsequent gene expression in SCs (Kao et al., 2009; Li et al., 2001). The HMG-domain transcription factor SOX10, which is essential for the generation of NCSCs from hPSCs, positively regulates the expression of the SC markers ErbB3 (Britsch et al., 2001), Krox20 (Kao et al., 2009), and S100β (Fujiwara et al., 2014), and functions as a central component of SC behaviors and specification (Britsch et al., 2001; Finzsch et al., 2010). A key feature of our protocol is the use of NRG1, a ligand of the HER/ErbB receptors, as a key trigger to access SC fate at a very early stage of transient neural induction (Figure 1A). In an early step of neuralization, the expression of SOX10 was significantly and dose-dependently induced by simply adding exogenous NRG1 (Figures 1C and 1D), accompanied by SC differentiation. These results indicate that NRG1-ErbB signaling is a key directional cue to drive SC fate specification of a plastic intermediate state of hPSC differentiation and that it depends on the function of SOX10.

We aggressively tested previously reported differentiation protocols, and, with slight modifications, directed differentiation of hPSC-SCPs to SCs was successfully produced by incubation with a combination of SC differentiation factors: NRG1, forskolin, RA, and PDGF-BB. Unfortunately, however, without exposure to fetal bovine serum (FBS) (1%–2%), hPSC-SCP-SCs were poorly differentiated and maintained. The hPSC-SCP-SCs were identified by the expression of SC-specific markers including S100β, MPZ, OCT6, SOX10, and NGFR, and by in vitro secretion of the neurotrophic factors BDNF, GDNF, NGF, and NT-3, which are critical for neuronal development, survival, and regeneration, and for the maintenance of the nervous system (Allen et al., 2013; Dezawa, 2002). Our hPSC-SCP-SCs in vitro secreted various neurotrophic factors, demonstrating the functionality of the SCs. Fully differentiated SCs were maintained in NRG1-supplemented culture medium for more than 3 months.

Co-culture with rat DRG neurons resulted in a tight association of hPSC-SCP-SCs with axons, suggesting myelination in vitro. Most of hPSC-SCP-SCs were positive for S100 and aligned with neurofilament-positive DRG neurons (Figure 4B). Based on the counts of MBP^+ cells, the frequency of myelinating hSCs, tightly localized along with axons, was much less. We therefore assume that the majority of hPSC-SCP-SCs are in pre-myelinating state. While a human and animal cell-based co-culture system is very useful to recapitulate the in vitro myelination, hSCs derived from different sources and methods led to an extremely low efficiency of in vitro myelination in co-cultures with rat DRG neurons (Lehmann et al., 2012; Liu et al., 2012; Morrissey et al., 1995; Sowa et al., 2017; Thoma et al., 2014), possibly due to the species differences. It is likely that the differences in myelination efficiency of different hSCs depend largely on rat DRG survival and proliferation, the cell-to-cell ratio, and the cell number during myelination induction. Thus, we believe that a human and human cell-based co-culture system using human neurons and SCs will more accurately recapitulate the features of human myelination and would provide even more insights into myelination or demyelination process.

In an in vivo study, the transplantation of hPSC-SCP-SCs into a sciatic nerve-injured mouse promoted nerve fiber regeneration, and the transplanted cells integrated into renewed axons (Figures 5 and S6). However, without SC transplantation, demyelinated axons and nerve defects were not restored (Figure S6C). These observations suggest that our myelin-generating hPSC-SCP-SCs contribute to the therapeutic effect of peripheral nerve regeneration through the release of neurotrophic factors that promote axonal growth. This report provides the evidence that hPSC-derived SCs, obtained via an intermediate step, SCPs, can give rise to myelinating SCs both in vitro as well as in vivo. Although the myelination capacity of hPSC-SCP-SCs appears to be low, and still needs to be improved, the self-renewing hPSC-SCPs promise a valuable resource to produce functional hSCs that can myelinate neurons both in vitro and in vivo.

Because SCs have the ability to myelinate CNS axons, transplantation of SCs has the potential to promote the regeneration of spinal nerves (Bachelin et al., 2005; Biernaskie et al., 2007; Kocsis and Waxman, 2007; Papastefanaki et al., 2007; Pearse et al., 2007). Thus, it is highly probable that our SCPs are applicable to cell therapy for repair in both the PNS and CNS, which we will investigate in future studies. When using the sciatic nerve-injured mouse model

system, there are limits to analyzing the potential contributions of exogenous and endogenous SCs to restore remyelination and nerve defects in detail. Further evaluation of the functionality and myelination capacity hPSC-SCP-SCs in a demyelination animal model such as shiverer mice (McKenzie et al., 2006) would be valuable to understand the mechanisms of demyelination and remyelination and to develop therapeutics to promote nerve regeneration.

Our work provides an efficient protocol for generating functional, clinical-grade SCs from patient- or disease-specific hPSCs via SCPs, which can easily be expanded and stored within a short period of time (Figure 6). Currently, hiPSCs generated from patient-derived cells have become an ideal source for combined cell and gene therapy, which is at the forefront of developing treatments for human disease. Thus, the application of patient- and disease-specific hPSCs from patients with SC-related genetic diseases and their derivatives, SCPs and SCs, into rapidly evolving stem cell and gene therapy approaches is highly desirable and offers hope for the development of future treatments.

EXPERIMENTAL PROCEDURES

Animals

Animal experiments were performed in accordance with the guidelines of the KRIBB Institutional Animal Care and Use Committee. The KRIBB Animal Welfare Assurance number was KRIBB-AEC-11039.

SCP Derivation from Human Pluripotent Stem Cells

For SCP derivation from hPSCs, the colonized hPSCs were re-plated onto growth factor-reduced Matrigel-coated culture dishes. The next day, the culture medium was switched from hPSC culture medium to NDM containing 1× N2, 1× B27, 0.005% BSA, 2 mM GlutaMAX, 0.11 mM β-mercaptoethanol, 3 μM CT 99021 (Tocris Biosciences), and 20 μM SB431542 (Tocris Biosciences) in advanced DMEM/F12 and Neurobasal medium (1:1 mix). After 6 days of differentiation, the medium was replaced with neural induction medium containing 50 ng/mL NRG1 (this is designated Schwann cell precursor differentiation medium [SCPDM]) and replaced with fresh medium daily. The cells were routinely dissociated with Accutase treatment upon reaching 80% confluence and were expanded by additional cultivation in SCPDM. The hPSC-derived SCPs were generated after approximately 18 days of differentiation. SCPDM was used for the induction and maintenance of hPSC-derived SCPs.

Differentiation of SCPs into Schwann Cells

For differentiation into SCs, SCPs were cultured on Matrigel-coated plates in SCDM containing 1% FBS, 200 ng/mL NRG1, 4 μM forskolin (Sigma), 100 nM all-*trans* RA (Sigma) and 10 ng/mL PDGF-BB in DMEM/low glucose. After 3 days of incubation, the culture medium was replaced with SCDM containing 1% FBS, 200 ng/mL NRG1, and 10 ng/mL PDGF-BB (Thermo Fisher Scientific), but not forskolin or RA. After another 2 days of incubation, the culture medium was replaced with SCDM containing 1% FBS and 200 ng/mL NRG1 but not forskolin, RA, or PDGF-BB (Schwann cell medium [SCM]). The cells were maintained in SCM for expansion. SCs were generated after approximately 2–3 days of incubation in SCM.

Statistical Analysis

The results are presented as the means ± SE. Student's unpaired t test was used for statistical evaluation, and $p < 0.01$ was considered significant.

ACCESSION NUMBERS

Microarray data in this article was deposited in the GEO under accession number GEO: GSE95004.

SUPPLEMENTAL INFORMATION

Supplemental Information includes Supplemental Experimental Procedures, six figures, and two tables and can be found with this article online at http://dx.doi.org/10.1016/j.stemcr.2017.04.011.

AUTHOR CONTRIBUTIONS

Conception and Design, Collection and/or Assembly of Data, Data Analysis and Interpretation, Manuscript Writing, and Final Approval of the Manuscript, H.S.K.; Collection and/or Assembly of Data, Data Analysis and Interpretation, J.L. and D.Y.L.; Collection and/or Assembly of Data, Y.D.K., J.Y.K., H.J.L., and S.L. Conception and Design, Financial Support, Data Analysis and Interpretation, Manuscript Writing, and Final Approval of the Manuscript, Y.S.C.

ACKNOWLEDGMENTS

We heartily thank Professor Hwan Tae Park of Dong-A University for advice and suggestions during this work. This work was supported by the National Research Foundation of Korea (NRF; 2012M3A9C7050224) and by the National Research Council of Science & Technology (NST) Grant from the Korean government (MSIP) (No. CRC-15-02-KRIBB).

Received: June 27, 2016
Revised: April 8, 2017
Accepted: April 10, 2017
Published: May 11, 2017

REFERENCES

Adameyko, I., Lallemend, F., Aquino, J.B., Pereira, J.A., Topilko, P., Muller, T., Fritz, N., Beljajeva, A., Mochii, M., Liste, I., et al. (2009). Schwann cell precursors from nerve innervation are a cellular origin of melanocytes in skin. Cell *139*, 366–379.

Al-Zer, H., Apel, C., Heiland, M., Friedrich, R.E., Jung, O., Kroeger, N., Eichhorn, W., and Smeets, R. (2015). Enrichment and Schwann cell differentiation of neural crest-derived dental pulp stem cells. In Vivo *29*, 319–326.

Allen, S.J., Watson, J.J., Shoemark, D.K., Barua, N.U., and Patel, N.K. (2013). GDNF, NGF and BDNF as therapeutic options for neurodegeneration. Pharmacol. Ther. *138*, 155–175.

Bacallao, K., and Monje, P.V. (2013). Opposing roles of PKA and EPAC in the cAMP-dependent regulation of Schwann cell proliferation and differentiation [corrected]. PLoS One *8*, e82354.

Bachelin, C., Lachapelle, F., Girard, C., Moissonnier, P., Serguera-Lagache, C., Mallet, J., Fontaine, D., Chojnowski, A., Le Guern, E., Nait-Oumesmar, B., et al. (2005). Efficient myelin repair in the macaque spinal cord by autologous grafts of Schwann cells. Brain *128*, 540–549.

Biernaskie, J., Sparling, J.S., Liu, J., Shannon, C.P., Plemel, J.R., Xie, Y., Miller, F.D., and Tetzlaff, W. (2007). Skin-derived precursors generate myelinating Schwann cells that promote remyelination and functional recovery after contusion spinal cord injury. J. Neurosci. *27*, 9545–9559.

Birchmeier, C., and Nave, K.A. (2008). Neuregulin-1, a key axonal signal that drives Schwann cell growth and differentiation. Glia *56*, 1491–1497.

Brennan, A., Dean, C.H., Zhang, A.L., Cass, D.T., Mirsky, R., and Jessen, K.R. (2000). Endothelins control the timing of Schwann cell generation in vitro and in vivo. Dev. Biol. *227*, 545–557.

Britsch, S., Goerich, D.E., Riethmacher, D., Peirano, R.I., Rossner, M., Nave, K.A., Birchmeier, C., and Wegner, M. (2001). The transcription factor Sox10 is a key regulator of peripheral glial development. Genes Dev. *15*, 66–78.

Chambers, S.M., Fasano, C.A., Papapetrou, E.P., Tomishima, M., Sadelain, M., and Studer, L. (2009). Highly efficient neural conversion of human ES and iPS cells by dual inhibition of SMAD signaling. Nat. Biotechnol. *27*, 275–280.

Chen, Z., Pradhan, S., Liu, C., and Le, L.Q. (2012). Skin-derived precursors as a source of progenitors for cutaneous nerve regeneration. Stem Cells *30*, 2261–2270.

Dezawa, M. (2002). Central and peripheral nerve regeneration by transplantation of Schwann cells and transdifferentiated bone marrow stromal cells. Anat. Sci. Int. *77*, 12–25.

Dong, Z., Sinanan, A., Parkinson, D., Parmantier, E., Mirsky, R., and Jessen, K.R. (1999). Schwann cell development in embryonic mouse nerves. J. Neurosci. Res. *56*, 334–348.

Dyachuk, V., Furlan, A., Shahidi, M.K., Giovenco, M., Kaukua, N., Konstantinidou, C., Pachnis, V., Memic, F., Marklund, U., Muller, T., et al. (2014). Neurodevelopment. Parasympathetic neurons originate from nerve-associated peripheral glial progenitors. Science *345*, 82–87.

Espinosa-Medina, I., Outin, E., Picard, C.A., Chettouh, Z., Dymecki, S., Consalez, G.G., Coppola, E., and Brunet, J.F. (2014). Parasympathetic ganglia derive from Schwann cell precursors. Science *345*, 87–90.

Falls, D.L. (2003). Neuregulins: functions, forms, and signaling strategies. Exp. Cell Res. *284*, 14–30.

Finzsch, M., Schreiner, S., Kichko, T., Reeh, P., Tamm, E.R., Bosl, M.R., Meijer, D., and Wegner, M. (2010). Sox10 is required for Schwann cell identity and progression beyond the immature Schwann cell stage. J. Cell Biol. *189*, 701–712.

Fujiwara, S., Hoshikawa, S., Ueno, T., Hirata, M., Saito, T., Ikeda, T., Kawaguchi, H., Nakamura, K., Tanaka, S., and Ogata, T. (2014). SOX10 transactivates S100B to suppress Schwann cell proliferation and to promote myelination. PLoS One *9*, e115400.

Golden, K.L., Pearse, D.D., Blits, B., Garg, M.S., Oudega, M., Wood, P.M., and Bunge, M.B. (2007). Transduced Schwann cells promote axon growth and myelination after spinal cord injury. Exp. Neurol. *207*, 203–217.

Jessen, K.R., and Mirsky, R. (2005). The origin and development of glial cells in peripheral nerves. Nat. Rev. Neurosci. *6*, 671–682.

Jessen, K.R., Brennan, A., Morgan, L., Mirsky, R., Kent, A., Hashimoto, Y., and Gavrilovic, J. (1994). The Schwann cell precursor and its fate: a study of cell death and differentiation during gliogenesis in rat embryonic nerves. Neuron *12*, 509–527.

Jiang, X., Gwye, Y., McKeown, S.J., Bronner-Fraser, M., Lutzko, C., and Lawlor, E.R. (2009). Isolation and characterization of neural crest stem cells derived from in vitro-differentiated human embryonic stem cells. Stem Cells Dev. *18*, 1059–1070.

Kao, S.C., Wu, H., Xie, J., Chang, C.P., Ranish, J.A., Graef, I.A., and Crabtree, G.R. (2009). Calcineurin/NFAT signaling is required for neuregulin-regulated Schwann cell differentiation. Science *323*, 651–654.

Kocsis, J.D., and Waxman, S.G. (2007). Schwann cells and their precursors for repair of central nervous system myelin. Brain *130*, 1978–1980.

Krause, M.P., Dworski, S., Feinberg, K., Jones, K., Johnston, A.P., Paul, S., Paris, M., Peles, E., Bagli, D., Forrest, C.R., et al. (2014). Direct genesis of functional rodent and human Schwann cells from skin mesenchymal precursors. Stem Cell Reports *3*, 85–100.

Kreitzer, F.R., Salomonis, N., Sheehan, A., Huang, M., Park, J.S., Spindler, M.J., Lizarraga, P., Weiss, W.A., So, P.L., and Conklin, B.R. (2013). A robust method to derive functional neural crest cells from human pluripotent stem cells. Am. J. Stem Cells *2*, 119–131.

Krishnan, A. (2013). Neuregulin-1 type I: a hidden power within Schwann cells for triggering peripheral nerve remyelination. Sci. Signal. *6*, jc1.

Lavasani, M., Thompson, S.D., Pollett, J.B., Usas, A., Lu, A., Stolz, D.B., Clark, K.A., Sun, B., Peault, B., and Huard, J. (2014). Human muscle-derived stem/progenitor cells promote functional murine peripheral nerve regeneration. J. Clin. Invest. *124*, 1745–1756.

Lee, G., Chambers, S.M., Tomishima, M.J., and Studer, L. (2010). Derivation of neural crest cells from human pluripotent stem cells. Nat. Protoc. *5*, 688–701.

Lehmann, H.C., Chen, W., Mi, R., Wang, S., Liu, Y., Rao, M., and Hoke, A. (2012). Human Schwann cells retain essential phenotype characteristics after immortalization. Stem Cells Dev. *21*, 423–431.

Levi, A.D., Guenard, V., Aebischer, P., and Bunge, R.P. (1994). The functional characteristics of Schwann cells cultured from human peripheral nerve after transplantation into a gap within the rat sciatic nerve. J. Neurosci. *14*, 1309–1319.

Li, Y., Tennekoon, G.I., Birnbaum, M., Marchionni, M.A., and Rutkowski, J.L. (2001). Neuregulin signaling through a PI3K/Akt/Bad pathway in Schwann cell survival. Mol. Cell. Neurosci. *17*, 761–767.

Li, W., Sun, W., Zhang, Y., Wei, W., Ambasudhan, R., Xia, P., Talantova, M., Lin, T., Kim, J., Wang, X., et al. (2011). Rapid induction and long-term self-renewal of primitive neural precursors from human embryonic stem cells by small molecule inhibitors. Proc. Natl. Acad. Sci. USA *108*, 8299–8304.

Liu, Q., Spusta, S.C., Mi, R., Lassiter, R.N., Stark, M.R., Hoke, A., Rao, M.S., and Zeng, X. (2012). Human neural crest stem cells derived from human ESCs and induced pluripotent stem cells: induction, maintenance, and differentiation into functional Schwann cells. Stem Cells Transl. Med. *1*, 266–278.

Liu, Q., Swistowski, A., and Zeng, X. (2014). Human neural crest stem cells derived from human pluripotent stem cells. Methods Mol. Biol. *1210*, 79–90.

Lobsiger, C.S., Smith, P.M., Buchstaller, J., Schweitzer, B., Franklin, R.J., Suter, U., and Taylor, V. (2001). SpL201: a conditionally immortalized Schwann cell precursor line that generates myelin. Glia *36*, 31–47.

Martens, W., Sanen, K., Georgiou, M., Struys, T., Bronckaers, A., Ameloot, M., Phillips, J., and Lambrichts, I. (2014). Human dental pulp stem cells can differentiate into Schwann cells and promote and guide neurite outgrowth in an aligned tissue-engineered collagen construct in vitro. FASEB J. *28*, 1634–1643.

McKenzie, I.A., Biernaskie, J., Toma, J.G., Midha, R., and Miller, F.D. (2006). Skin-derived precursors generate myelinating Schwann cells for the injured and dysmyelinated nervous system. J. Neurosci. *26*, 6651–6660.

Menendez, L., Yatskievych, T.A., Antin, P.B., and Dalton, S. (2011). Wnt signaling and a Smad pathway blockade direct the differentiation of human pluripotent stem cells to multipotent neural crest cells. Proc. Natl. Acad. Sci. USA *108*, 19240–19245.

Monje, P.V., Athauda, G., and Wood, P.M. (2008). Protein kinase A-mediated gating of neuregulin-dependent ErbB2-ErbB3 activation underlies the synergistic action of cAMP on Schwann cell proliferation. J. Biol. Chem. *283*, 34087–34100.

Monje, P.V., Soto, J., Bacallao, K., and Wood, P.M. (2010). Schwann cell dedifferentiation is independent of mitogenic signaling and uncoupled to proliferation: role of cAMP and JNK in the maintenance of the differentiated state. J. Biol. Chem. *285*, 31024–31036.

Morrissey, T.K., Kleitman, N., and Bunge, R.P. (1995). Human Schwann cells in vitro. II. Myelination of sensory axons following extensive purification and heregulin-induced expansion. J. Neurobiol. *28*, 190–201.

Ndubaku, U., and de Bellard, M.E. (2008). Glial cells: old cells with new twists. Acta Histochem. *110*, 182–195.

Newbern, J., and Birchmeier, C. (2010). Nrg1/ErbB signaling networks in Schwann cell development and myelination. Semin. Cell Dev. Biol. *21*, 922–928.

Papastefanaki, F., Chen, J., Lavdas, A.A., Thomaidou, D., Schachner, M., and Matsas, R. (2007). Grafts of Schwann cells engineered to express PSA-NCAM promote functional recovery after spinal cord injury. Brain *130*, 2159–2174.

Pearse, D.D., Sanchez, A.R., Pereira, F.C., Andrade, C.M., Puzis, R., Pressman, Y., Golden, K., Kitay, B.M., Blits, B., Wood, P.M., et al. (2007). Transplantation of Schwann cells and/or olfactory ensheathing glia into the contused spinal cord: survival, migration, axon association, and functional recovery. Glia *55*, 976–1000.

Razavi, S., Zarkesh-Esfahani, H., Morshed, M., Vaezifar, S., Karbasi, S., and Golozar, M.A. (2015). Nanobiocomposite of poly(lactide-co-glycolide)/chitosan electrospun scaffold can promote proliferation and transdifferentiation of Schwann-like cells from human adipose-derived stem cells. J. Biomed. Mater. Res. A *103*, 2628–2634.

Ren, Y.J., Zhang, S., Mi, R., Liu, Q., Zeng, X., Rao, M., Hoke, A., and Mao, H.Q. (2013). Enhanced differentiation of human neural crest stem cells towards the Schwann cell lineage by aligned electrospun fiber matrix. Acta Biomater. *9*, 7727–7736.

Rutkowski, J.L., Kirk, C.J., Lerner, M.A., and Tennekoon, G.I. (1995). Purification and expansion of human Schwann cells in vitro. Nat. Med. *1*, 80–83.

Sakaue, M., and Sieber-Blum, M. (2015). Human epidermal neural crest stem cells as a source of Schwann cells. Development *142*, 3188–3197.

Smith, J.R., Vallier, L., Lupo, G., Alexander, M., Harris, W.A., and Pedersen, R.A. (2008). Inhibition of Activin/Nodal signaling promotes specification of human embryonic stem cells into neuroectoderm. Dev. Biol. *313*, 107–117.

Sowa, Y., Kishida, T., Tomita, K., Yamamoto, K., Numajiri, T., and Mazda, O. (2017). Direct conversion of human fibroblasts into Schwann cells that facilitate regeneration of injured peripheral nerve in vivo. Stem Cells Transl. Med. *6*, 1207–1216.

Thoma, E.C., Merkl, C., Heckel, T., Haab, R., Knoflach, F., Nowaczyk, C., Flint, N., Jagasia, R., Jensen Zoffmann, S., Truong, H.H., et al. (2014). Chemical conversion of human fibroblasts into functional Schwann cells. Stem Cell Reports *3*, 539–547.

Tomita, K., Madura, T., Sakai, Y., Yano, K., Terenghi, G., and Hosokawa, K. (2013). Glial differentiation of human adipose-derived stem cells: implications for cell-based transplantation therapy. Neuroscience *236*, 55–65.

Woodhoo, A., and Sommer, L. (2008). Development of the Schwann cell lineage: from the neural crest to the myelinated nerve. Glia *56*, 1481–1490.

Xiao, Y.Z., and Wang, S. (2015). Differentiation of Schwann-like cells from human umbilical cord blood mesenchymal stem cells in vitro. Mol. Med. Rep. *11*, 1146–1152.

Xu, Y., Liu, L., Li, Y., Zhou, C., Xiong, F., Liu, Z., Gu, R., Hou, X., and Zhang, C. (2008). Myelin-forming ability of Schwann cell-like cells induced from rat adipose-derived stem cells in vitro. Brain Res. *1239*, 49–55.

Ziegler, L., Grigoryan, S., Yang, I.H., Thakor, N.V., and Goldstein, R.S. (2011). Efficient generation of Schwann cells from human embryonic stem cell-derived neurospheres. Stem Cell Rev. *7*, 394–403.

Stem Cell Reports, Volume *8*

Supplemental Information

Schwann Cell Precursors from Human Pluripotent Stem Cells as a Potential Therapeutic Target for Myelin Repair

Han-Seop Kim, Jungwoon Lee, Da Yong Lee, Young-Dae Kim, Jae Yun Kim, Hyung Jin Lim, Sungmin Lim, and Yee Sook Cho

Supplemental Information

Schwann cell precursors from human pluripotent stem cells a potential therapeutic target for myelin repair

Han-Seop Kim, Jungwoon Lee, Da Yong Lee, Young-Dae Kim, Jae Yun Kim, Hyung Jin Lim, Sungmin Lim, and Yee Sook Cho

Figure S1

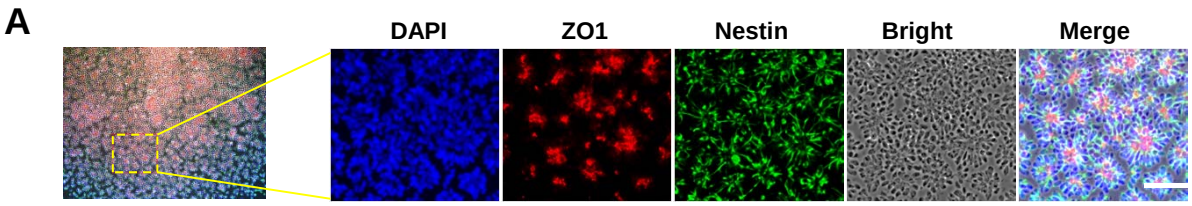

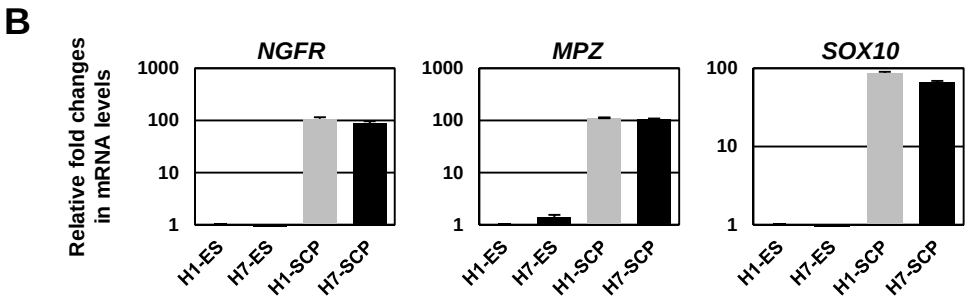

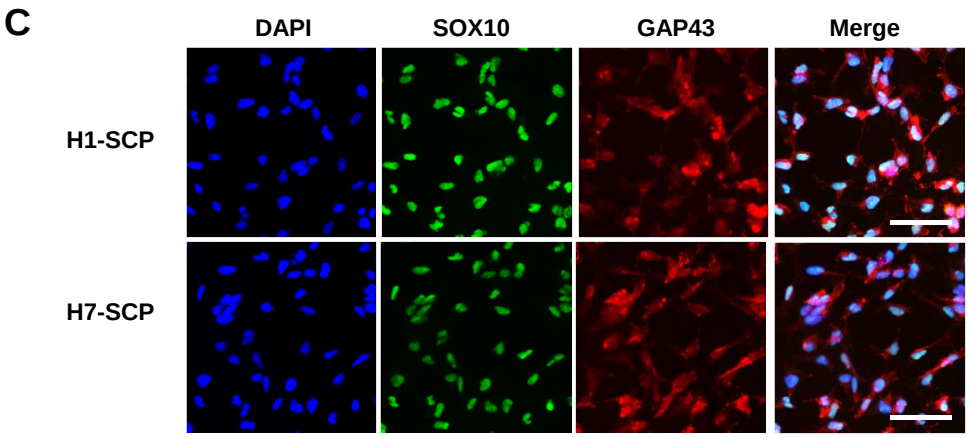

D

Medium condition	Results
SB+CT+NRG1	Expandable
SB+CT	Not expandable
SB+NRG1	Not expandable
CT+NRG1	Not expandable
NRG1	Not expandable
No treatment	Not expandable

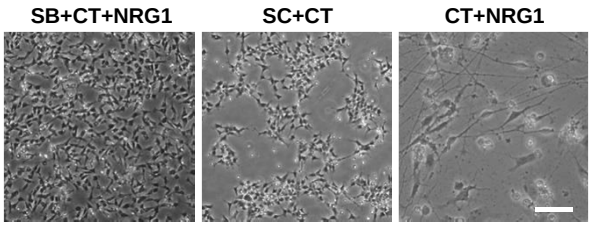

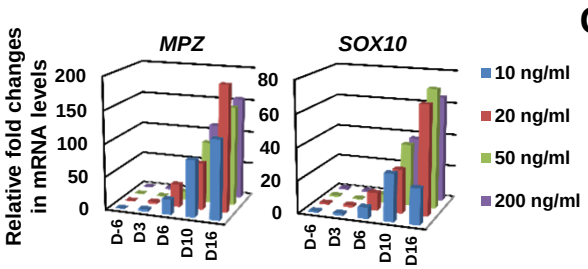

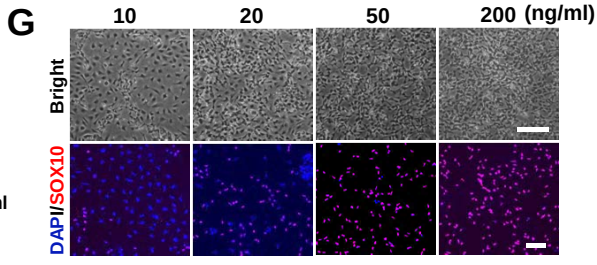

Figure S1, related to Figure 1. NRG1 and two small molecules, CT and SB, are required for the generation of hSCPs from hPSCs. (A) Representative images showing neural rosettes stained immunocytochemically for Nestin (green) and ZO1 (red) at D0, where H9 hESCs were treated with neural differentiation medium (NDM) for 6 days. DAPI (blue) was used to stain the cell nuclei. Scale bars = 100 μm. (B) Expression analysis of SCP marker genes (*CDH19, MPZ,* and *SOX10*) in H1 hESCs, H7 hESCs, H1 hESC-SCPs, and H7 hESC-SCPs, was performed using qPCR. Mean ± SE (n=3 independent experiments). (C) Immunocytochemical staining for SOX10 (green) and GAP43 (red) at differentiation day 24. DAPI (blue) was used to stain the cell nuclei. Scale bars = 100 μm. (D) Scalable generation of hSCPs from hPSCs (hESCs and hiPSCs) established by combined treatment with NRG1 and two small molecules, SB431542 (SB), CT99021 (CT). Under our differentiation conditions, individual omission of NRG1, SB, or CT from the medium resulted in a failure to generate hSCPs. (E) Representative bright-field images showing day 11 of differentiation from hESCs into hSCPs when the differentiation medium lacked an individual compound such as NRG1 or SB. Scale bars = 100 μm. (F) qPCR analysis of SCP markers (*MPZ* and *SOX10*) during the process of hSCP induction by treatment with various concentrations of NRG1. (G) Representative bright-field images showing day 14 of differentiation from hESCs into hSCPs. Immunostaining showing that the number of SOX10-positive cells was dependent on the concentration of NRG1 at day 14 post-differentiation. Cell nuclei were stained with DAPI (blue). Scale bars = 100 μm.

Figure S2

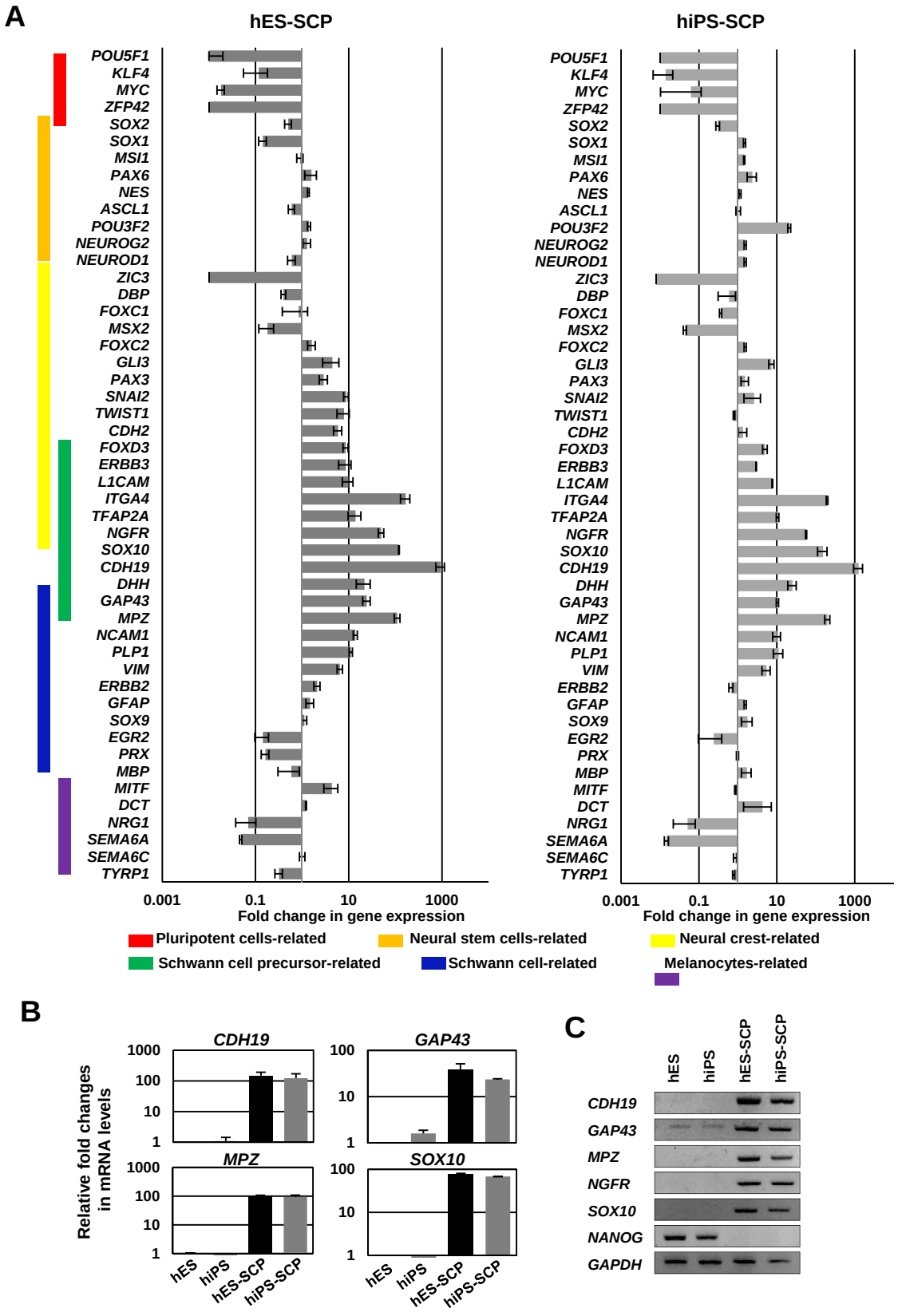
A
hES-SCP
hiPS-SCP
POU5F1
KLF4
MYC
ZFP42
SOX2
SOX1
MSI1
PAX6
NES
ASCL1
POU3F2
NEUROG2
NEUROD1
ZIC3
DBP
FOXC1
MSX2
FOXC2
GLI3
PAX3
SNAI2
TWIST1
CDH2
FOXD3
ERBB3
L1CAM
ITGA4
TFAP2A
NGFR
SOX10
CDH19
DHH
GAP43
MPZ
NCAM1
PLP1
VIM
ERBB2
GFAP
SOX9
EGR2
PRX
MBP
MITF
DCT
NRG1
SEMA6A
SEMA6C
TYRP1
0.001
0.1
10
1000
Fold change in gene expression
Pluripotent cells-related
Neural stem cells-related
Neural crest-related
Schwann cell precursor-related
Schwann cell-related
Melanocytes-related
B
Relative fold changes in mRNA levels
CDH19
GAP43
MPZ
SOX10
1000
100
10
1
hES
hiPS
hES-SCP
hiPS-SCP
C
hES
hiPS
hES-SCP
hiPS-SCP
CDH19
GAP43
MPZ
NGFR
SOX10
NANOG
GAPDH

Figure S2, related to Figure 1. Gene array analysis of hPSC-SCPs. (A) Expression levels (fold change) of genes associated with pluripotent cells, neural stem cells, neural crest cells, Schwann cell precursors, Schwann cells and melanocytes were compared between H9-SCPs and hiPSC-SCPs). Microarray analysis was performed at day 29 post-SCP differentiation. All values are relative to undifferentiated hESCs (day -6). Mean ± SE (n=2 independent experiments). Expression analysis of SCP marker genes (*CDH19, GAP43, MPZ,* and *SOX10*) in H9 hESCs, hiPSCs, hESC-SCPs, and hiPSC-SCPs, was performed using qPCR (B) and semi-quantitative RT-PCR (C). Mean ± SE (n=3 independent experiments).

Figure S3

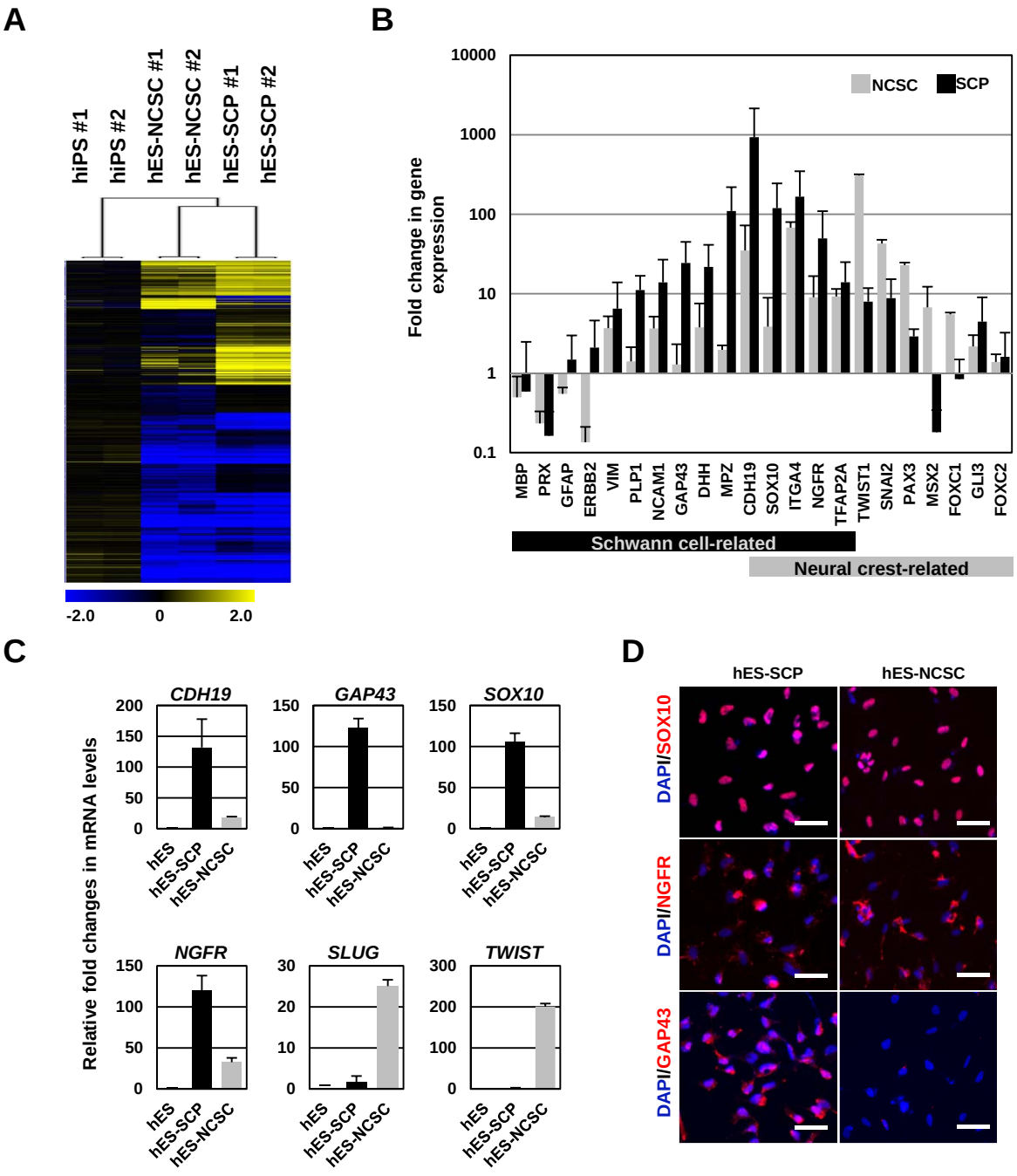
A
hiPS #1
hiPS #2
hES-NCSC #1
hES-NCSC #2
hES-SCP #1
hES-SCP #2
-2.0
0
2.0
B
NCSC
SCP
Fold change in gene expression
10000
1000
100
10
1
0.1
MBP
PRX
GFAP
ERBB2
VIM
PLP1
NCAM1
GAP43
DHH
MPZ
CDH19
SOX10
ITGA4
NGFR
TFAP2A
TWIST1
SNAI2
PAX3
MSX2
FOXC1
GLI3
FOXC2
Schwann cell-related
Neural crest-related
C
Relative fold changes in mRNA levels
CDH19
GAP43
SOX10
NGFR
SLUG
TWIST
hES
hES-SCP
hES-NCSC
D
hES-SCP
hES-NCSC
DAPI/SOX10
DAPI/NGFR
DAPI/GAP43

Figure S3, related to Figure 1. Characterization of hPSC-SCPs: comparison of hSCPs and hNCSCs. (A) Hierarchical clustering of the dataset of genes showing significantly differential expression (3,666 significant transcripts (one-way ANOVA, $p<0.01$)) in six samples: 2 hiPSC lines, 2 H9-NCSC lines (hNCSCs), and 2 H9-SCP lines (hSCPs). Heat map indicating the relative value of the log10 fold change normalized to the undifferentiated H9-hESCs. (B) Gene array analysis in both H9-NCSCs (hNCSCs) and H9-SCPs (hSCPs). Expression levels (fold change) of genes associated with Schwann cells and neural crest are shown compared to those of undifferentiated hESCs (day -6). Mean ± SE (n=3 independent experiments). (C) qPCR analysis of SCP markers and NCSC markers in H9 hESCs, hSCPs and hNCSCs. (D) Immunocytochemical analysis of hSCPs and hNCSCs using SOX10 (red), NGFR (red), and GAP43 (red). Cell nuclei were stained with DAPI (blue). Scale bars = 50 μm.

Figure S4

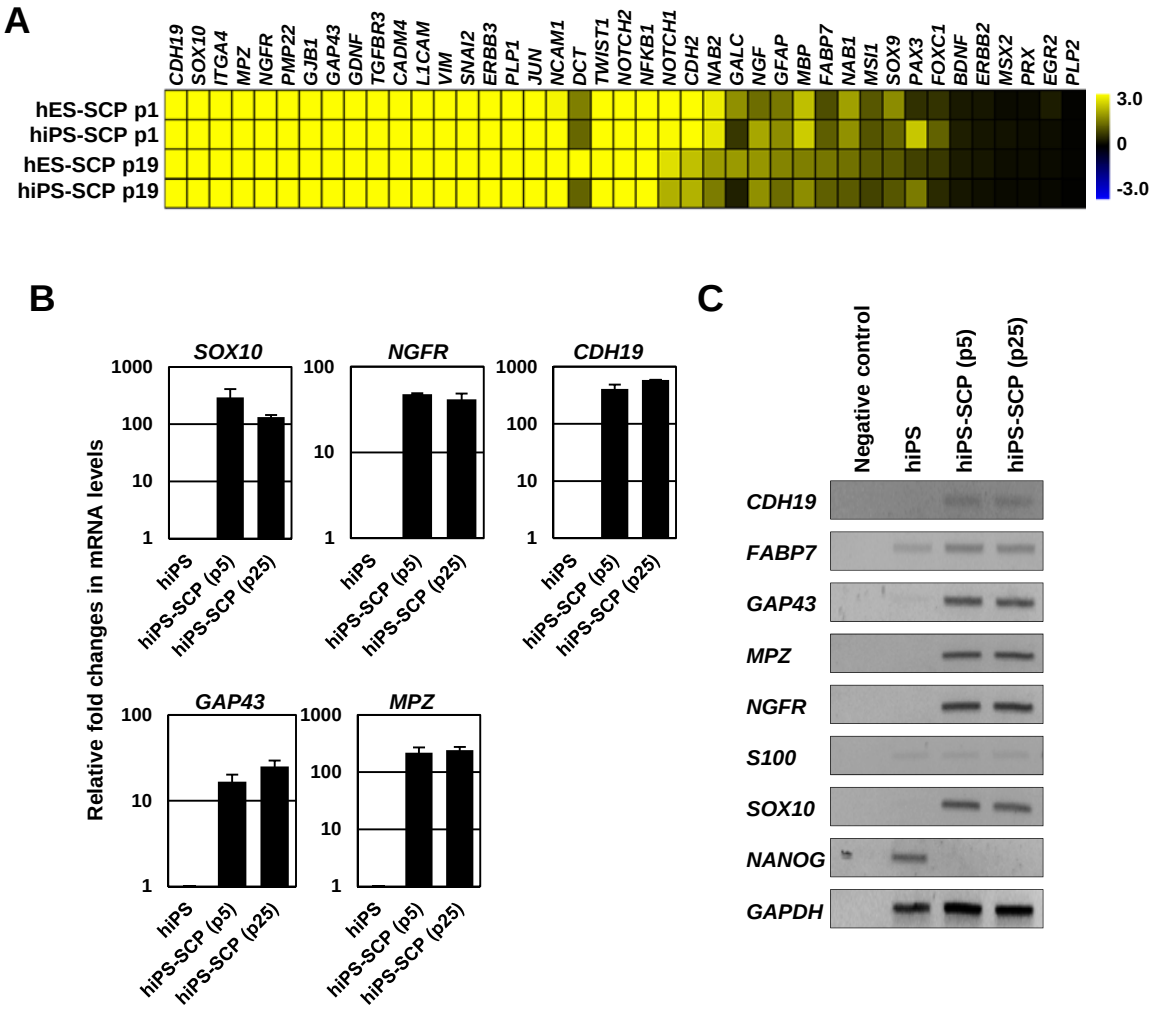

Figure S4, related to Figure 2. hSCPs are self-renewing and maintain hSCP properties after long-term culture. (A) Microarray analysis of early-passage hSCPs (p1) and long-term cultured (late-passage) hSCPs (p19) from H9 hESCs. Heat map indicating the relative value of the log10 fold change based on the value determined for undifferentiated hESCs. qPCR (B) and RT-PCR (C) analysis of early-passage (p5) hSCPs and late-passage (p25) hSCPs using SCP markers (*CDH19, GAP43, ITGA4, MPZ, NGFR,* and *SOX10*). Mean ± SE (n=4 independent experiments).

Figure S5

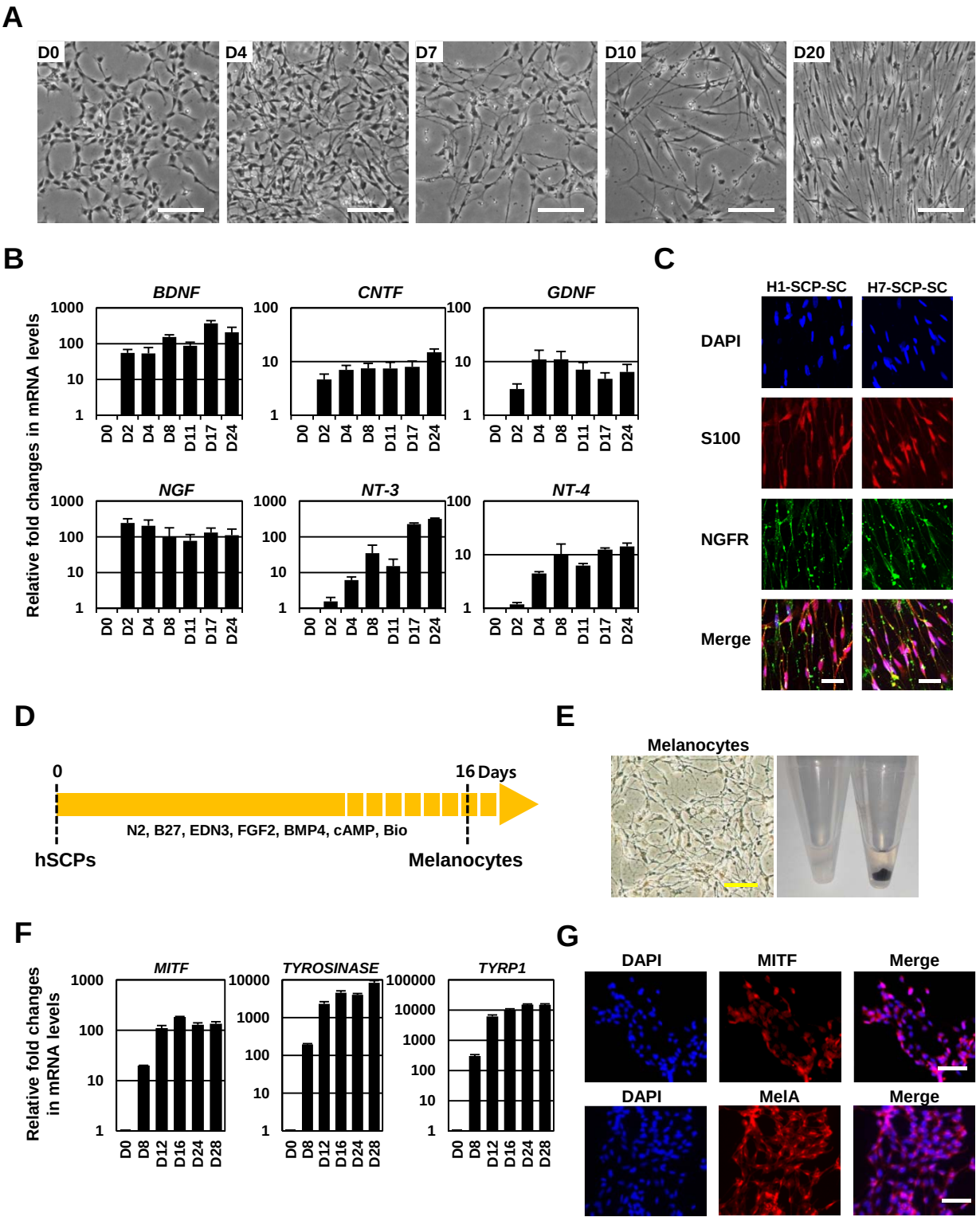
A
D0
D4
D7
D10
D20
B
BDNF
CNTF
GDNF
NGF
NT-3
NT-4
Relative fold changes in mRNA levels
1000
100
10
1
D0 D2 D4 D8 D11 D17 D24
C
H1-SCP-SC
H7-SCP-SC
DAPI
S100
NGFR
Merge
D
0
16 Days
N2, B27, EDN3, FGF2, BMP4, cAMP, Bio
hSCPs
Melanocytes
E
Melanocytes
F
MITF
TYROSINASE
TYRP1
Relative fold changes in mRNA levels
D0 D8 D12 D16 D24 D28
G
DAPI
MITF
Merge
DAPI
MelA
Merge

Figure S5, related to Figure 3. hSCPs can efficiently and rapidly differentiate into Schwann cells. (A) Representative bright-field images showing the process of differentiation from hSCPs into Schwann cells at day 0, day 4, day 7, day 10, and day 20. Scale bar = 100 μm. (B) qPCR analysis of the neurotrophic factor genes *BDNF, CNTF, GDNF, NGF, NT-3,* and *NT-4* during hSCP-derived Schwann cell differentiation. Mean ± SE (n=4 independent experiments). (C) Immunostaining for the Schwann cell markers NGFR (green) and S100 (red) after 18 days of differentiation. Cell nuclei were stained with DAPI (blue). Scale bars = 100 μm. (D) H9-SCPs were differentiated into melanocytes using differentiation medium containing EDN3, FGF2, cAMP, Wnt and BMP4 signaling factors, and differentiated cells became pigmented within 16 days. (E) Left panel, representative bright-field image of differentiated cells at day 16. Right panel, the cell pellets in the right tube were completely pigmented, unlike the undifferentiated hSCPs in the left tube. (F) qPCR analysis of the melanogenesis-related genes *MITF, TYR,* and *TYRP1* during the differentiation of SCP-derived melanocytes. Mean ± SE (n=3 independent experiments). (G) Immunocytochemical analysis of hSCP-derived melanocytes using the melanocyte markers MITF (red) and MelA (red). Cell nuclei were stained with DAPI (blue). Scale bars = 100 μm.

Figure S6

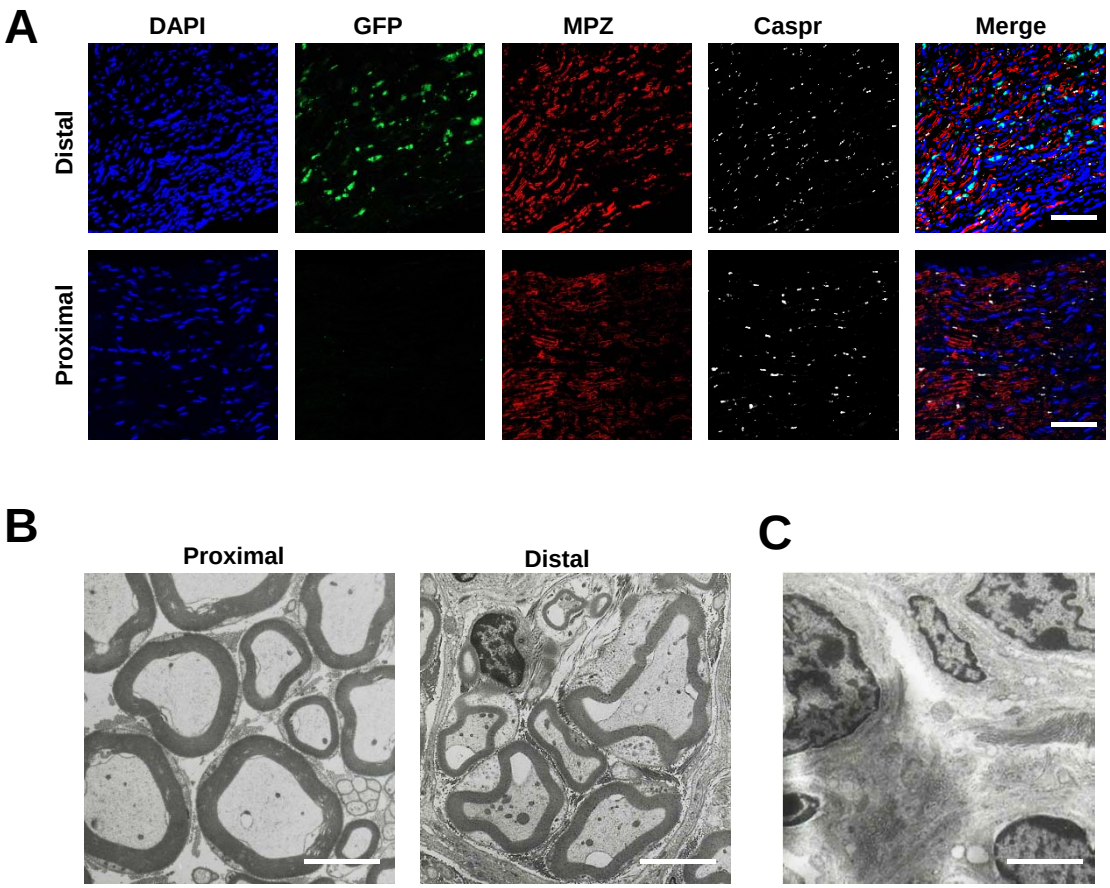

Figure S6, related to Figure 5. hSCP-SCs were integrated into regenerated sciatic nerves of the transplanted mice. (A) Representative image of a longitudinal section of a nerve induced to regenerate by H9-SCP-SCs, with immunostaining for MPZ (red) and CASPR (white). Cell nuclei were stained with DAPI (blue). The most grafted- GFP-labeled Schwann cells were observed in the distal region. Scale bars = 200 μm. (B) TEM images showing that the transplantation of SCP-SCs regenerated distal nerves as a complete remyelination bundle like the proximal regions. Scale bars = 5 μm. (C) A control TEM image showing demyelinated axons in distal region without SCP-SC transplantion. Scale bar = 5 μm.

Table S1. Primers for qRT-PCR

Gene	**Sequence (5'-->3')**	
PAX3	*Forward*	*AGC TCG GCG GTG TTT TTA TCA*
	Reverse	*CTG CAC AGG ATC TTG GAG ACG*
TWIST	*Forward*	*GTC CGC AGT CTT ACG AGG AG*
	Reverse	*GCT TGA GGG TCT GAA TCT TGC T*
SOX10	*Forward*	*CCT CAC AGA TCG CCT ACA CC*
	Reverse	*CAT ATA GGA GAA GGC CGA GTA GA*
FOXD3	*Forward*	*GAC GCA GGT TGC GAT AGC C*
	Reverse	*CGC CTC CTT GGG CAA TGT C*
MPZ	*Forward*	*AAG TGC CAA CTA GGT ACG GG*
	Reverse	*CAT AGC ACT GAG CCT CCT CT*
CDH19	*Forward*	*ACA AGC GTC TGT AAC TCT GGG*
	Reverse	*AGC AAA CTT CGT GTT GGA CA*
NGFR	*Forward*	*TGG CCT ACA TAG CCT TCA AGA*
	Reverse	*GAG ATG CCA CTG TCG CTG T*
GAP43	*Forward*	*GGC CGC AAC CAA AAT TCA GG*
	Reverse	*CGG CAG TAG TGG TGC CTT C*
NANOG	*Forward*	*CTC AGC CTC CAG CAG ATG C*
	Reverse	*TAG ATT TCA TTC TCT GGT TCT GG*
GAPDH	*Forward*	*ACA ACT TTG GTA TCG TGG AAG G*
	Reverse	*GCC ATC ACG CCA CAG TTT C*
SLUG	*Forward*	*CGA ACT GGA CAC ACA TAC AGT G*
	Reverse	*CTG AGG ATC TCT GGT TGT GGT*
FABP7	*Forward*	*GCA CAT TCA AGA ACA CGG AGA*
	Reverse	*CAC ATC ACC AAA AGT AAG GGT CA*
S100	*Forward*	*GAC CCT CAT CAA CGT GTT CCA*
	Reverse	*CCA CAA GCA CCA CAT ACT CCT*
SOX17	*Forward*	*GTG GAC CGC ACG GAA TTT G*
	Reverse	*GGA GAT TCA CAC CGG AGT CA*
GFAP	*Forward*	*AGG TCC ATG TGG AGC TTG AC*
	Reverse	*GCC ATT GCC TCA TAC TGC GT*
EGR2	*Forward*	*TCT TCC CAA TGA TCC CAG ACT*
	Reverse	*TTA CGG ATT GTA GAG AGT GGA GT*
NGF	*Forward*	*GGC AGA CCC GCA ACA TTA CT*
	Reverse	*CAC CAC CGA CCT CGA AGT C*
PMP22	*Forward*	*GAT CCT GTC GAT CAT CTT CAG C*

	Reverse	*AGC ACT CAT CAC GCA CAG AC*
PLP	*Forward*	*ACC TAT GCC CTG ACC GTT G*
	Reverse	*TGC TGG GGA AGG CAA TAG ACT*
ITGA4	*Forward*	*AGC CCT AAT GGA GAA CCT TGT*
	Reverse	*CCA GTG GGG AGC TTA TTT TCA T*
BDNF	*Forward*	*CTA CGA GAC CAA GTG CAA TCC*
	Reverse	*AAT CGC CAG CCA ATT CTC TTT*
TYROSINASE	*Forward*	*GCA AAG CAT ACC ATC AGC TCA*
	Reverse	*GCA GTG CAT CCA TTG ACA CAT*
MITF	*Forward*	*CTC ACA GCG TGT ATT TTT CCC A*
	Reverse	*ACT TTC GGA TAT AGT CCA CGG AT*
TYRP1	*Forward*	*CCC TGG ATA TGG CAA AGC G*
	Reverse	*CCT GTC CTA CCC CAA GGA AAG*

Table S2. List of antibodies

Protein	**Company (Cat. No.)**	**Dilution**
SOX10	Abcam (AB155279)	1:200
SOX10	Bioss (bs-6449R-A488)	1:200
SOX10	R&D (MAB2864)	1:50
NGFR	Abcam (AB3125)	1:50
NGFR	Bioss (bs-0161R-A647)	1:200
TUJ-1	Covance (MRB-435P)	1:1000
NF	Abcam (ab24575)	1:1000
GAP43	Abcam (AB75810)	1:500
GAP43	Bioss (bs-0154R-A647)	1:100
Nestin	Abcam (AB290)	1:1000
ZO-1	Thermo Fisher (40-2300)	1:100
GFP	Abcam (AB290)	1:1000
MPZ	Abcam (AB31851)	1:100
MPZ	Abcam (AB39375)	1:100
MPZ	Bioss (bs-0337R-A488)	1:100
EGR2	Abcam (AB156765)	1:100
MBP	Millipore (MAB386)	1:300
S100b	Abcam (AB52642)	1:200
Ki67	BD (550609)	1:50
MITF	Santa Cruz (SC56726)	1:100
MelA	Abcam (AB140503)	1:100
hNU	Millipore(MAB1281)	1:50

Supplemental Experimental Procedures

Maintenance of Human Pluripotent Stem Cells

H1, H7, and H9 hESCs (WiCell Research Institute) and hiPSCs derived from human newborn foreskin fibroblasts (catalog number CRL-2097; ATCC) (Son et al., 2014) were cultured as described previously (Son et al., 2013). For feeder-free cultures, cells were grown on dishes coated with growth factor-reduced Matrigel (BD Biosciences) in mTeSR1 medium (StemCell Technologies) with daily medium changes.

NCSC Derivation from Human Pluripotent Stem Cells

NCSCs were derived from hPSCs was performed as previously described(Menendez et al., 2013). Briefly, the dissociated hPSCs were plated onto Matrigel-coated culture dishes. The next day, the culture medium was replaced with NCSC induction medium (NCSCIM) containing 1% Probumin (Millipore), 1% penicillin-streptomycin, 1% L-alanyl-L-glutamine (Cellgro), 1% MEM non-essential amino acids, 0.1% trace elements A (Cellgro), 0.1% trace elements B (Cellgro), 0.1% trace elements C (Cellgro), 0.11 mM β-mercaptoethanol, 10 μg/ml transferrin, 50 μg/ml (+)-sodium l-ascorbate (Sigma), 10 ng/ml NRG1 (Peprotech), 200 ng/ml LONG R3 IGF-I (Sigma), 3 μM BIO (Tocris Biosciences), 20 μM SB431542 (Tocris Biosciences) and 8 ng/ml FGF2 (Peprotech). The culture medium was changed every day. NCSCs were generated after approximately 20 days of growth in NCSCIM. Unless otherwise indicated, all reagents were purchased from Thermo Fisher Scientific.

Differentiation of SCPs into Melanocytes

Differentiation into melanocytes was performed as previously described with appropriate modifications(Chambers et al., 2013). Briefly, SCPs were cultured on Matrigel-coated culture dishes. The next day, the culture medium was replaced with melanocyte derivation medium containing 1x N2, 1x B27, 0.005% BSA, 2 mM Glutamax, 0.11 mM β-mercaptoethanol, 3 μM CT 99021, 20 ng/ml FGF2 (Peprotech), 0.5 mM dbcAMP (Tocris Biosciences), 25 ng/ml BMP4, and 100 nM EDN3 (Tocris Biosciences) in advanced DMEM/F12 and Neurobasal medium (1:1 mix). The medium was replaced every other day. The confluent cells were dissociated using Accutase (Millipore) treatment and passaged at 1:6.

Preparation of Primary Schwann Cells

For comparison, primary human Schwann cells were purchased from ScienCell and cultured in Schwann cell growth medium (ScienCell).

Quantitative RT-PCR.

Total RNA was extracted from cultured cells using the RNeasy Mini Kit following the manufacturer's instructions. RNA (2 μg) was reverse-transcribed using the SuperScript® VILO™ cDNA Synthesis Kit according to the manufacturer's instructions (Thermo Fisher Scientific). Quantitative polymerase chain reaction (qPCR) was performed with SYBR green and analyzed using the 7500 Fast Real-Time PCR system (Thermo Fisher Scientific). The primers used are described in Supplementary (Table S1).

Immunocytochemistry.

Cells were fixed with 4% paraformaldehyde in PBS for 10 min, and DRG co-cultured cells were fixed with cold methanol for 15 min. The fixed cells were washed with PBS four times for 10 min each and then blocked and permeabilized with 0.3% Triton X-100, 10% FBS, and

1% BSA in PBS for 1 hour at room temperature. The cells were incubated with primary antibody in PBS containing 2% BSA for 1 hour at room temperature. After the primary antibody reaction, the cells were washed with PBS three times and incubated for 20 min at room temperature in PBS containing 2% BSA with Alexa 488-conjugated anti-mouse (1:500, Thermo Fisher Scientific), Alexa 546-conjugated anti-mouse (1:500, Thermo Fisher Scientific), Alexa 488-conjugated anti-rabbit (1:500, Thermo Fisher Scientific), Cy3-conjugated anti-rat (1:500, Thermo Fisher Scientific) or Alexa 546-conjugated anti-rabbit (1:500, Thermo Fisher Scientific) secondary antibodies. Fluorescent images were obtained using an Axio Vert.A1 microscope (Carl Zeiss) and LSM800 confocal microscope (Carl Zeiss).

Flow Cytometry

The cultured cells were dissociated with Accutase and resuspended in PBS. The cells were fixed with 4% formaldehyde in PBS for 10 min and washed with PBS 3 times. The fixed cells were blocked and permeabilized with 0.1% Triton X-100, 10% FBS, and 1% BSA in PBS for 1 hour on ice. The cells were incubated with fluorophore-conjugated primary antibody (Table S2) in PBS containing 2% BSA for 10 min at room temperature. Unconjugated SOX10 antibody (Abcam) was detected using anti-rabbit Alexa Fluor 488-conjugated secondary antibody as shown in Figure 1. Isotype control rabbit IgG (Abcam) were used for negative controls for FACS gating. After the antibody reaction, the cells were washed twice with PBS and analyzed using a BD Accuri C6 (BD Biosciences)

Microarrays and Analyses

Total RNA was extracted using an RNeasy Mini kit and labeled with Cy3. According to the manufacturer's protocols, the labeled RNA was hybridized to an Agilent Human GE 4x44K Microarray chip (one-color platform) (Agilent). After washing, the chip was placed in a slide holder and scanned using an Agilent C scanner. The gene expression data were processed using GeneSpring software (Agilent). For statistical analysis and to visualize the significance of each sample, we used MeV v.4.9.0 software.

Enzyme-linked Immunosorbent Assay (ELISA)

To obtain conditioned medium, 10^5 cells of hSCPs and hSCP-SCs in 2 ml were seeded on a 30-mm culture dish. After 48 hours, the cultured medium was filtered through a 0.22-μm filter (Millipore). To determine the concentration of secreted neurotrophic factors (BDNF, GDNF, b-NGF, and NT-3), ELISAs were performed using the conditioned medium derived from hSCPs and hSCP-SCs according to the manufacturer's protocol (Abcam).

Animals

Animal experiments were performed in accordance with the guidelines of the KRIBB Institutional Animal Care and Use Committee. The KRIBB Animal Welfare Assurance number was KRIBB-AEC-11039.

In Vitro Myelination

Dorsal root ganglion (DRG) neurons were prepared from rat pups at embryonic day 15. The DRGs were pre-plated on coverslips coated with poly-D-lysine and laminin in DRG growth medium [MEM and 15% FBS supplemented with 4 g/L D-glucose (Sigma), 50 ng/ml NGF

(Peprotech)] at a density of 10,000 cells *per* well of a 24-well plate (or 20,000 cells *per* well of a 12-well plate). To eliminate non-neuronal cells, the cultures were treated with 10 μM uridine (Sigma) and 10 μM 5-fluoro-2-deoxyuridine (Sigma), 4 g/L D-glucose (Sigma), 50 ng/ml NGF (Peprotech), 1% FBS, and 1x B27 in Neurobasal Medium for 3 days and then cultured in DRG growth medium for 2 days. This step was repeated 3 times. Purified DRG neurons were then maintained in DRG differentiation medium containing 4 g/L D-glucose (Sigma), 50 ng/ml NGF, 1% FBS, and 1x B27 in Neurobasal Medium before co-culturing with Schwann cells. The SCP-derived Schwann cells (SCP-SCs) were plated onto DRG neurons at a density of 20,000 cells *per* well of a 24-well plate (40,000 cells *per* well of a 12-well plate) in DRG differentiation medium and maintained for 7 days. The *in vitro* myelination of DRG neurons by SCP-SCs was induced by addition of 50 ng/ml ascorbic acid (Sigma) for 3 weeks. DRG differentiation medium was refreshed every day. SCP-SCs and DRGs co-cultures were fixed and analyzed by immunofluorescent staining with antibodies against MBP, S100B, NF, and MPZ. The proportion of myelinated DRG neurons were assesses by manually counting the total number of MBP-positive cells *per* well (n=16)

Cell Transplantation, In Vivo Myelination, and Sciatic Nerve Function index

The sciatic nerves of 8-week-old C57BL/6 male mice were injured by cutting the central region of the left sciatic nerve to create an approximately 2-3-mm nerve defect due to nerve retraction. Prior to transplantation, H9-SCPs were infected with pWPXL-GFP lentivirus and then GFP-labeled cells were differentiated into SCP-SCs for 2 weeks. These differentiated cells were diluted in Matrigel (2 x 104 cells/μl), and 5 μl of cell suspension containing 1 x 105 cells was implanted at the site of the nerve defect.

To determine the *in vivo* myelination efficacy, we analyzed the GFP- and MBP-

positive cells in 60 slices of regenerated sciatic nerves, which sliced longitudinally from 3 sciatic nerves. The GFP-expressing transplanted human SCP-SCs and their immunofluorescence reactivity for MBP were analyzed using confocal microscopy. The proportion of MBP-positive cells in GFP-positive cells was quantitated by counting 6 randomly selected fields among distal region of 60 slices.

Quantitative *in vivo* functional recovery was evaluated by recording the footprint and calculating the sciatic function index (SFI), which are methods used to assess nerve recovery after sciatic nerve injury (Inserra et al., 1998). Briefly, the hind paws were painted with ink, and then the mice were allowed to walk along a corridor (length 80 cm, width 6 cm) lined with white papers. Footprints were obtained at 2, 3, 4, 6, and 8 weeks after sciatic nerve injury. The collected footprints were scanned, and 3 parameters (PL, distance from the heel to the third toe, TS, distance from the first to the fifth toe, and ITS, distance from the second to the fourth toe) were measured using a ruler. All measurements were obtained from the experimental paw (EPL, ETS, and EITS) and from the uninjured paw (NPL, NTS, and NITS) of each mouse. SFI was calculated using the following formula:

SFI = -38.3 x (EPL-NPL)/NPL + 109.5 x (ETS-NTS)/NTS + 13.3 x (EITS-NITS)/NITS – 8.8.

Immunohistochemistry and Transmission Electron Microscopy (TEM)

Mice were perfused transcardially with 4% paraformaldehyde in PBS. The sciatic nerves were post-fixed for 1 hour and then cryoprotected in 30% sucrose in PBS for 72 h at 4 °C. Cryostat sections (15 μm) were mounted on glass slides and stored at -20 °C. For immunostaining, the slides were washed with PBS for 15 min and then blocked with 0.3% Triton X-100, 10% FBS, and 1% BSA in PBS for 1 hour at room temperature. The primary antibodies were diluted in PBS containing 2% BSA and applied overnight at 4 °C. The slides

were washed with PBS and incubated with secondary antibodies for 45 min at room temperature. The images were obtained using an Axio Vert.A1 microscope (Carl Zeiss) and LSM800 confocal microscope (Carl Zeiss).

For TEM, mice were perfused transcardially with PBS. The sciatic nerves were fixed with 2.5% glutaraldehyde in PBS for 16 hours at 4 °C and then postfixed in 1% OsO4 in PBS for 4 hours at 4 °C. The specimens were dehydrated in an ascending series of ethanol and embedded in epoxy resin. Thin (80 nm) nerve cross-sections were cut with an ultramicrotome and observed using a transmission electron microscope.

Supplemental References

Chambers, S.M., Mica, Y., Lee, G., Studer, L., and Tomishima, M.J. (2013). Dual-SMAD Inhibition/WNT Activation-Based Methods to Induce Neural Crest and Derivatives from Human Pluripotent Stem Cells. Methods Mol Biol.

Inserra, M.M., Bloch, D.A., and Terris, D.J. (1998). Functional indices for sciatic, peroneal, and posterior tibial nerve lesions in the mouse. Microsurgery *18*, 119-124.

Menendez, L., Kulik, M.J., Page, A.T., Park, S.S., Lauderdale, J.D., Cunningham, M.L., and Dalton, S. (2013). Directed differentiation of human pluripotent cells to neural crest stem cells. Nat Protoc *8*, 203-212.

Son, M.Y., Choi, H., Han, Y.M., and Cho, Y.S. (2013). Unveiling the critical role of REX1 in the regulation of human stem cell pluripotency. Stem Cells *31*, 2374-2387.

Son, M.Y., Seol, B., Han, Y.M., and Cho, Y.S. (2014). Comparative receptor tyrosine kinase profiling identifies a novel role for AXL in human stem cell pluripotency. Hum Mol Genet *23*, 1802-1816.